AD-751 655

PREPARATION AND CHARACTERIZATION OF POLY-CRYSTALLINE HALIDES FOR USE IN HIGH POWER LASER WINDOWS

E. Bernal G., et al

Honeywell, Incorporated

Prepared for:

Advanced Research Projects Agency

15 October 1972

PREPARATION AND CHARACTERIZATION OF POLYCRYSTALLINE HALIDES FOR USE IN HIGH POWER LASER WINDOWS

E. Bernal G., Principal Investigator 612/332-5200 Ext. 8535
B. G. Koepke, Project Scientist 612/332-5200 Ext. 8530
R. H. Anderson, Project Scientist 612/332-5200 Ext. 8457
R. J. Stokes, Department Manager/Consultant 612/332-5200 Ext. 8525

HONEYWELL INC.
CORPORATE RESEARCH CENTER
10701 Lyndale Avenue, Bloomington, Minn. 55420

Quarterly Technical Report No. 2

1 July 1972 to 30 September 1972

CONTRACT NO. DAHC15-72-C-0227
EFFECTIVE DATE OF CONTRACT 1 April 1972
CONTRACT EXPIRATION DATE 31 DECEMBER 1972
AMOUNT OF CONTRACT $77,250

SPONSORED BY

Advanced Research Projects Agency
ARPA Order No. A02172; Program Code No. P-2D10

HR-72-286:5-26

UNCLASSIFIED

Security Classification

DOCUMENT CONTROL DATA - R & D

(Security classification of title, body of abstract and indexing annotation must be entered when the overall report is classified)

1 ORIGINATING ACTIVITY (Corporate author)	2a. REPORT SECURITY CLASSIFICATION
Honeywell Inc. Corporate Research Center	Unclassified
	2b. GROUP --

3 REPORT TITLE

Preparation and Characterization of Polycrystalline Halides for Use in High Power Laser Windows

4 DESCRIPTIVE NOTES (Type of report and inclusive dates)

Quarterly Technical Report #2 - 1 July to 30 September 1972

5 AUTHOR(S) (First name, middle initial, last name)

E. Bernal G., R. J. Stokes, B. G. Koepke, R. H. Anderson

6 REPORT DATE	7a. TOTAL NO. OF PAGES	7b. NO OF REFS
October 15, 1972	~~59~~ 67	15

8a. CONTRACT OR GRANT NO	9a. ORIGINATOR'S REPORT NUMBER(S)
DAHC15-72-C-0227 b. PROJECT NO Program Code No. P2D10 c. d.	HR-72-286:5-26 9b. OTHER REPORT NO(S) (Any other numbers that may be assigned this report)

10 DISTRIBUTION STATEMENT

This document is subject to special export controls and each transmittal to foreign governments or foreign nationals may be made only with prior approval of Advanced Research Projects Agency.

11 SUPPLEMENTARY NOTES	12 SPONSORING MILITARY ACTIVITY
--	ARPA - Materials Science Office

13 ABSTRACT

The mechanisms of high temperature deformation of alkali halides are reviewed. It is shown that at high temperatures it is possible to deform these materials to an arbitrary shape without void formation. The practical implementation of methods for hot working halides to produce strengthened polycrystalline bodies are described. The mechanical, microstructural and optical properties of polycrystalline potassium chloride produced are presented. The mechanical strength of the polycrystalline material is about 8X higher than that of the single crystal. A stable microstructure of ~5μm diameter grains can be produced. However, excessive deformation can produce abnormal grain growth at room temperature. The optical absorption of the hot worked materials is essentially unchanged from that of the starting single crystals. Some results of interferometric measurements of laser-induced deformation are presented. An expression for the temperature rise produced by irradiation of a low absorption sample by a laser beam is given.

DD FORM 1 NOV 68 1473 REPLACES DD FORM [illegible] WHICH IS OBSOLETE FOR [illegible]

UNCLASSIFIED

Security Classification

14

KEY WORDS	LINK A		LINK B		LINK C	
	ROLE	WT	ROLE	WT	ROLE	WT
Alkali Halides						
Lasers						
Infrared						
Polycrystalline						
Interferometry						
Calorimetry						
Forging						
Extrusion						

PREPARATION AND CHARACTERIZATION OF POLYCRYSTALLINE HALIDES FOR USE IN HIGH POWER LASER WINDOWS

E. Bernal G., Principal Investigator 612/332-5200 Ext. 8535
B. G. Koepke, Project Scientist 612/332-5200 Ext. 8530
R. H. Anderson, Project Scientist 612/332-5200 Ext. 8457
R. J. Stokes, Department Manager/Consultant 612/332-5200 Ext. 8525

HONEYWELL INC.
CORPORATE RESEARCH CENTER
10701 Lyndale Avenue, Bloomington, Minn. 55420

Quarterly Technical Report No. 2

1 July 1972 to 30 September 1972

CONTRACT NO. DAHC15-72-C-0227
EFFECTIVE DATE OF CONTRACT 1 April 1972
CONTRACT EXPIRATION DATE 31 DECEMBER 1972
AMOUNT OF CONTRACT $77,250

SPONSORED BY

Advanced Research Projects Agency
ARPA Order No. A02172; Program Code No. P-2D10

HR-72-286:5-26

TABLE OF CONTENTS

LIST OF ILLUSTRATIONS

LIST OF ILLUSTRATIONS (Concluded)

INTRODUCTION

This program is concerned with the preparation and characterization of polycrystalline halides and their optical evaluation. Previous work has shown that fully dense polycrystalline material of various shapes can be obtained by the deformation and recrystallization of single crystals[1]; presently we are concerned with methods of producing shapes suitable for high power laser windows and the effect of processing on their properties.

SECTION I

HIGH TEMPERATURE DEFORMATION AND RECRYSTALLIZATION OF ALKALI HALIDES

This section gives a very brief background review of the macroscopic and microscopic aspects of the deformation and recrystallization of alkali halides.

A. EFFECT OF TEMPERATURE ON DEFORMATION MODE

The crystallographic features of the rock salt crystal structure restrict slip to taking place in the $<110>$ direction (Figure I-1). At low temperatures the ionic bonding character also restricts slip to the $\{110\}$ planes. The six variations of the $<110>$ $\{110\}$ low temperature slip parameters yield only two independent slip systems with the result that a single crystal is constrained to certain changes in shape.[2] This is referred to as plastic anisotropy and means that the single crystal cannot undergo a perfectly general change in shape, such as the distortions imposed by a complex fabrication procedure.[3]

At high temperatures (above~Tm /2) the restriction on slip planes disappears and shear occurs with equal facility over $\{110\}$, $\{100\}$, and $\{111\}$ planes. The increased flexibility available with these slip parameters yields five independent slip systems which means the five components of the strain tensor can be varied independently. This provides the necessary conditions for complete plasticity. Thus, at high enough temperatures (typically over 250°C for NaCl and 200°C for KCl) single crystals can undergo any change in shape without void formation. This further leads to the possibility that alkali halides can be hot worked and extruded to form rods, hot forged to form discs or hot rolled to form sheets. The exact temperatures and operating conditions depend on the material and method of fabrication.

It is found that single crystals which have undergone complex deform ation at high temperatures tend to recrystallize to give a fully dense polycrystalline material. material.[1, 4] The polycrystalline material has mechanical properties superior to the single crystal.[1] For this reason high temperature deformation and recrystallization has formed the basis for much of the present effort on the preparation of polycrystalline halides by the processing of single crystals.

B. MECHANISM OF RECRYSTALLIZATION

The origin of recrystallization following complex deformation can be appreciated from the microscopic aspects of flow in these materials. The dislocations responsible for plastic flow have as their Burgers vector $\frac{a}{2}$ <110>. These vectors intersect either at 90° (conjugate slip) or at 60° (oblique slip) as shown in Figure I-1. A conjugate dislocation reaction of the type

$$\frac{a}{2}[110] + \frac{a}{2}[1\bar{1}0] \rightarrow a[100] \qquad (1)$$

is not favored since there is no lowering of the dislocation strain energy, whereas an oblique reaction of the type

$$\frac{a}{2}[110] + \frac{a}{2}[\bar{1}0\bar{1}] \rightarrow \frac{a}{2}[01\bar{1}] \qquad (2)$$

is favored energetically. Figure I-2 depicts the consequence of this reaction in which the two dislocations (S_1E_1) and (S_2E_2) have united along the <111> direction to form (E_3E_3). This represents an elemental component of a dislocation network which, when extended over large areas, takes the form depicted in Figure I-3. These sub-grain structures were first studied and analyzed in detail for KCl by Amelinckz.[5] (An example of a network in MgO is reproduced in Figure I-4.) As high temperature deformation continues to

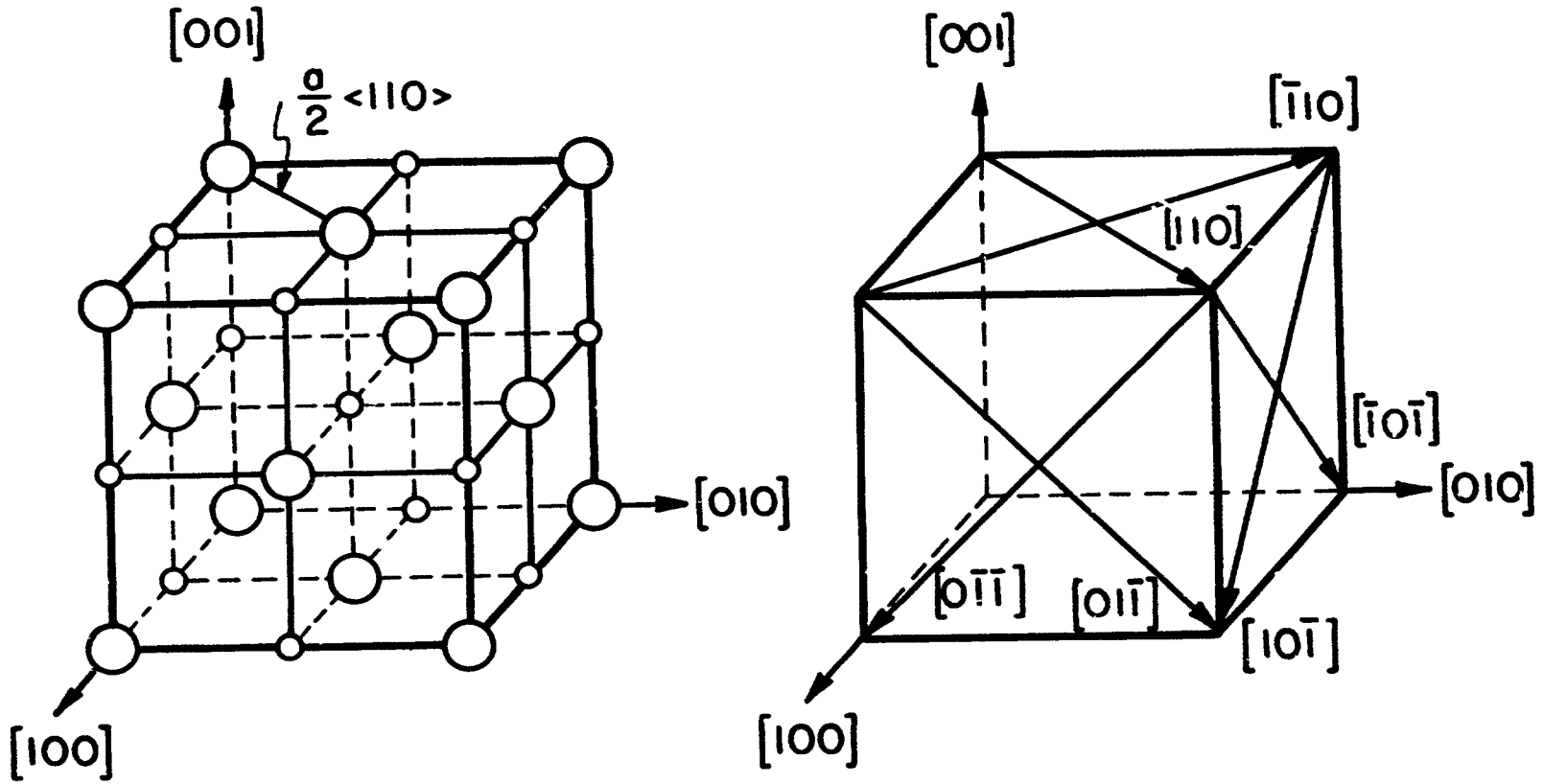

Figure I-1. Slip directions in the rock salt crystal structure. There are six $\frac{a}{2}$ < 110 > Burgers vectors.

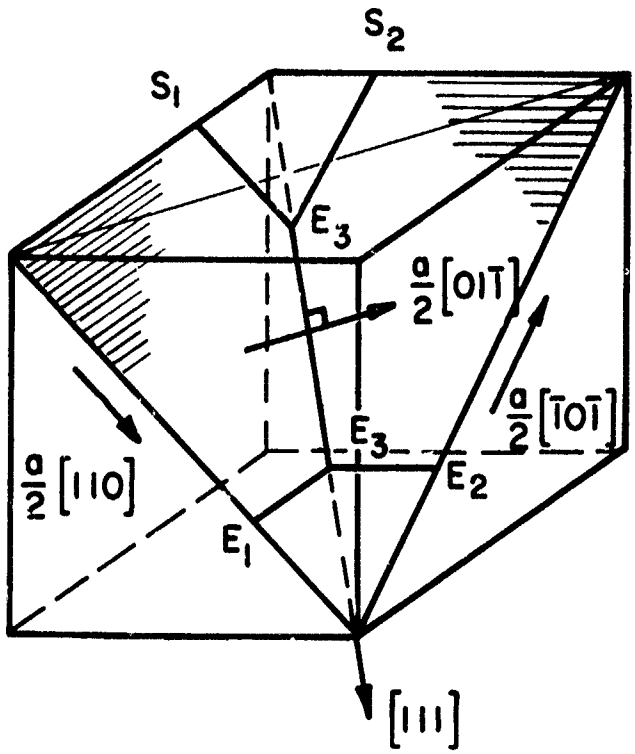

Figure I-2. The oblique dislocation reaction. Dislocations $S_1 E_1$ and $S_2 E_2$ have reacted to form a third dislocation along $E_3 E_3$. S-screw dislocation component, E-Edge dislocation component.

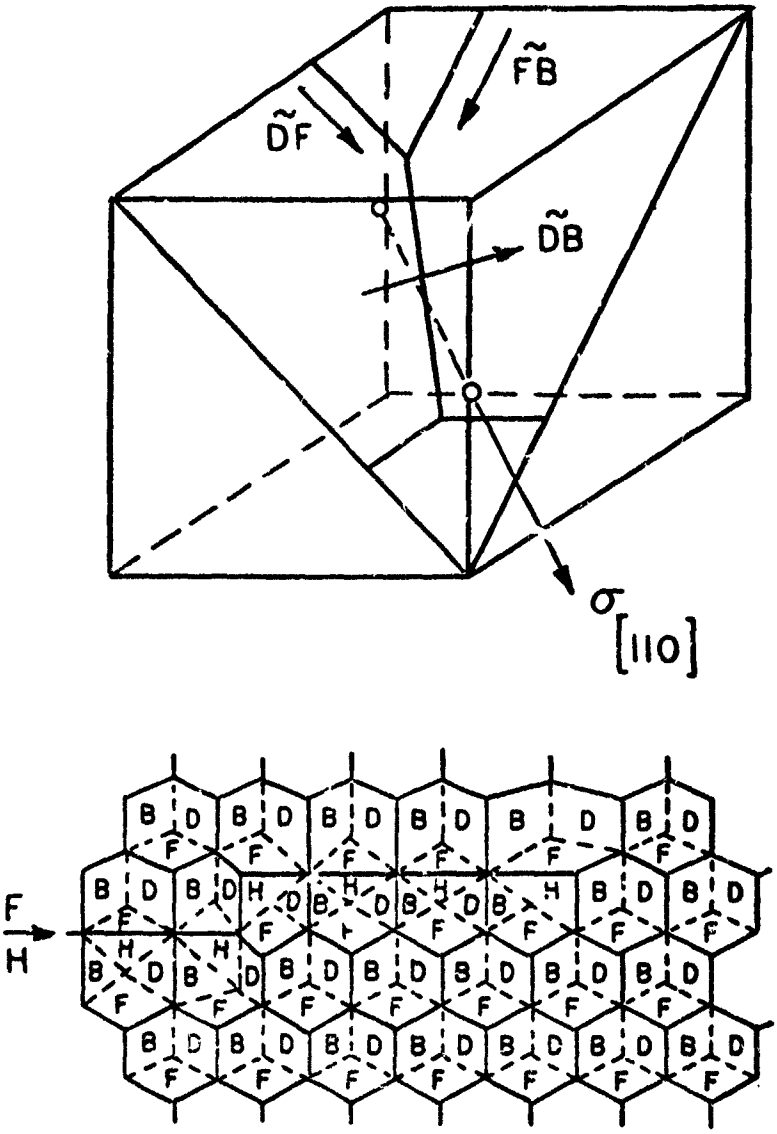

Figure I-3. The formation of dislocation networks in rock salt crystals.

$$\tilde{DF} + \tilde{FB} \rightarrow \tilde{DB}$$

The solid lines in the lower figure represent dislocation lines, with Burgers vectors denoted by letters on each side. The figure shows the change in onfiguration induced by the absorption of dislocation $\tilde{FH}$.

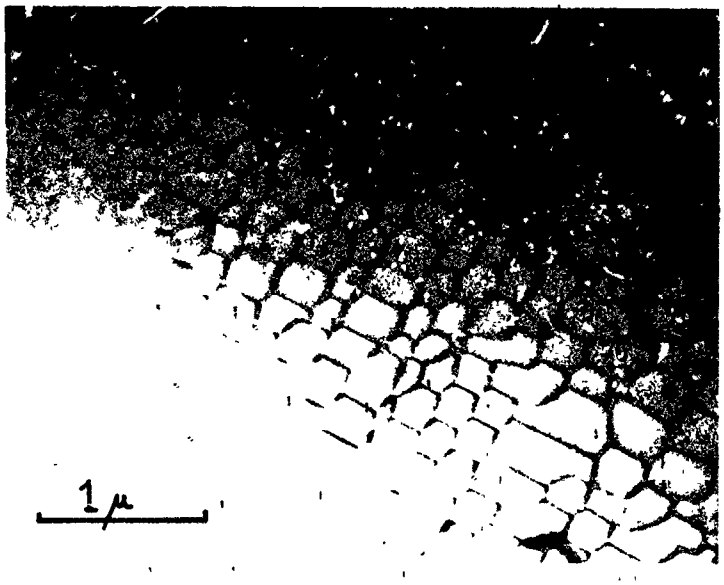

Figure I-4. Transmission electron micrograph of dislocation network in rock salt structure material, magnesium oxide.

higher strains more dislocations are pumped into these networks; dislocation rearrangement and climb occurs and a point is reached where the misorien tation across the subgrain boundary is large enough for it to be considered a grain boundary. The original single crystal then becomes broken down into a polycrystalline aggregate of the kind illustrated in Figure I-5. It should be noted that this recrystallization is not due to a cold work plus annealing treatment, but rather a consequence of the high temperature flow process. Extensive studies of this phenomena in magnesium oxide have demonstrated that the oblique dislocation reaction of equation (2), is essential for 'recrystallization'. Thus, recrystallization is favored by the complex strain conditions imposed by extrusion, forging and rolling.

At large strains and high temperatures a material can continuously recrystallize as a means of relieving the internal stress built up during deformation. The internal stress at any instant is the net result of two competing processes; strain hardening which tends to increase the internal stress and dynamic (stress activated) recovery and recrystallization which tends to decrease the internal stress. In any hot working operation both processes occur simultaneously. If the rate of hardening exceeds the rate of recovery high residual stresses will result, and there will be dislocation residue within the grains of the kind to be seen in Figure I-5. Both the as-worked grain size and the dislocation residue in the grains will depend upon the strain rate and temperature.

Annealing after fabrication can result in both static recovery (dislocation rearrangement by glide and climb) which can clean up the residue to form a more stable structure with lower residual stresses and recrystallization which results in a completely new strain free matrix.

Figure I-5. Transmission electron micrograph illustrating grain boundaries, subgrain boundaries and residual dislocations in recrystallized magnesium oxide single crystals.

C. FABRICATION METHODS

As indicated earlier, the increased slip flexibility and the relief of internal stresses by dislocation rearrangement and recrystallization afford the opportunity to fabricate polycrystalline halides by extrusion, forging and rolling. We have examined or are in the process of examining all three methods for the case of potassium chloride and its alloys.[6] It is our experience that potassium chloride becomes so plastic above 200°C that it will flow into any reentrant surface or small surface imperfection that is impressed upon it by a loading surface. One of the intrinsic advantages of the extrusion and rolling methods is that the processed material is projected free from any contact with a loading surface. The preparation of crack-free rods of polycrystalline KCl at 200°C by extrusion is a very straightforward process that provides fully dense samples.

The major problem to be overcome in hot forging is that the material remains in contact with the loading platens after fabrication. The large thermal contraction of potassium chloride relative to the loading platen material causes severe cracking unless the surface of the loading platens is perfectly smooth and unless there is a release agent to separate the potassium chloride from the loading platen.

After experimenting with different platen materials we have obtained the most satisfactory results with a ground steel platen surface lubricated with silicone oil (Dow Corning 200, 1000 cp viscosity).

SECTION II

PROCESSING TECHNIQUES, STRUCTURES, AND MECHANICAL PROPERTIES

A. PRESS FORGINGS

1. Experimental Procedure

a. Pressings -- All press forgings made to date have been produced in a hydraulic press having a maximum capacity of 500,000 pounds. A schematic of the press is shown in Figure II-1. The load on the billet is supplied by the upper ram whose motion is followed by an LVDT connected to a Honeywell Elektronik 19 strip chart recorder.

The billet is situated between two ground steel platens and is heated with a molydbenum element resistance furnace. The furnace, platens, and sample are surrounded with a water cooled vacuum chamber routinely kept at a pressure of 10 microns during a run. As mentioned earlier, silicone fluids have been found to be the most suitable platen lubricants. A slight depression has been machined in each platen to prevent the billet from sliding during pressing. The temperature is monitored with a Cr-Al thermocouple situated in a hole drilled into the top platen such that the thermocouple is one inch away from the sample.

After processing, the sample is removed as rapidly as possible from the furnace to keep the amount of post forming annealing to a minimum. Typically, a sample pressed at 175°C is at 50°C within five minutes following termination of the pressing.

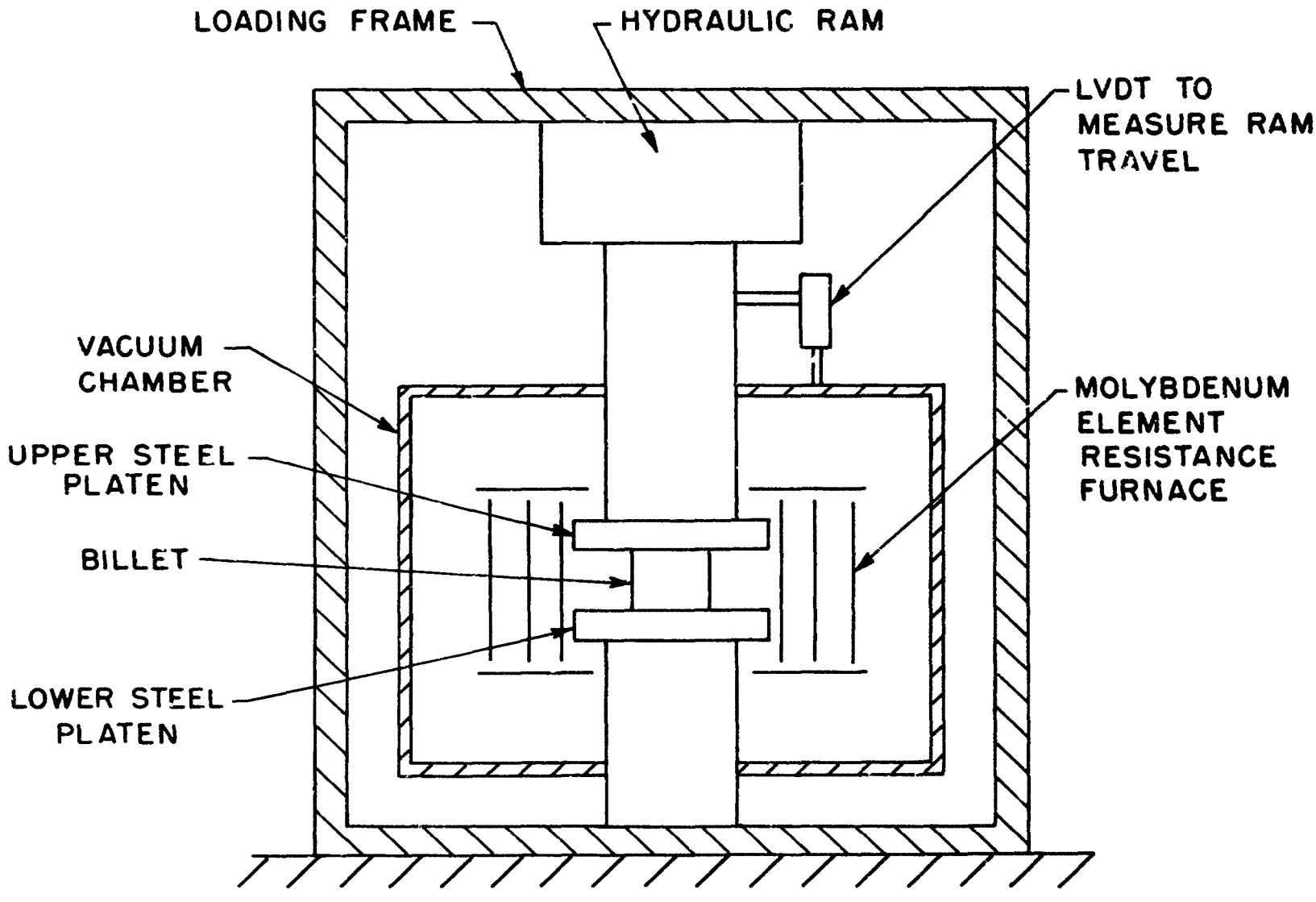

Figure II-1. Schematic of hydraulic press used to press forge KCl crystals.

b. Metallographic, Bend Test, and Texture Specimen Preparation -- The metallographic technique used in this study to examine the microstructures of KC1 forgings is based on that used by Grant et. al.[7] The samples are first cut from the forgings with a saw that utilizes a fine stainless steel wire continuously moistened with water as the cutting element. Following cutting, the surface to be examined is rough "ground" on a piece of silk moistened with water and stretched over a glass plate. At this time a considerable amount of material is generally removed to eliminate damage (if any) introduced by the sawing operation. The surface is then lightly abraded on a metallographic polishing wheel covered with silk and moistened with water. The sample is then thoroughly rinsed with alcohol and dried in a blast of Freon. At this time the surface is fairly flat, but does usually contain some scratches. Intermediate polishing is accomplished with a 50 percent methanol, 50 percent distilled water solution on a wheel covered with billiard cloth. Final polishing is carried out on the same wheel using 100 percent methanol. The surface is then etched by lightly rubbing the sample across the (stationary) billiard cloth surface slightly moistened with the 50 percent methanol, 50 percent distilled water solution and then quickly dried in the Freon blast. Surfaces produced in this manner are suitable for metallographic examination, but do have slightly rounded edges.

Bend test samples are produced by first hand lapping blanks cut with the wire saw roughly to shape on silk stretched on a glass plate and moistened with water. The samples are then immersion polished in cold water, rinsed with alcohol and ether, and tested. In all cases, the direction of surface finishing is along the long direction of the sample. Rice[8] has clearly shown the mechanical properties of bend test samples to be highest when finished in this manner.

c. Texture Determination -- Textures were determined with a Siemens pole figure goniometer using MoKα radiation. All texture determinations were made on water polished surfaces cut parallel to the top and bottom faces of a pressing

situated midway through the thickness. In most cases the region examined was near the (radial) center of the pressing.

2. Recent Forging Results

The following paragraphs discuss the results obtained on two groups of press forgings. One group was pressed to a reduction in thickness of approximately 60 percent (true strain = -.92) and the other was pressed to approximately 80 percent reduction in thickness (true strain = -1.61). In all pressings the initial billet was a KC1 crystal approximately 1.5 inches high and 1.5 inches in diameter. All were pressed in a < 100 > direction using a constant ram speed of .012 inches/minute (initial strain rate $\tilde{}$ .008 $min.^{-1}$) Pressings were carried out at 150°, 175° and 200°C.

Following pressing, the microstructure, texture, and mechanical strength of each pressing was characterized. These pressings are also currently undergoing an optical evaluation that is discussed later in this report.

Results obtained on the 60 percent pressings will be presented first followed by those obtained on the 80 percent pressings. A short description of some interesting structural instabilities observed in the 80 percent pressings will then be presented.

a. Crystals Pressed to 60 Percent Reduction in Thickness -- True stress-true strain curves obtained during the pressing of three KC1 crystals to approximately 60 percent reduction in height at 150°C, 175°C, and 200°C are shown in Figure II-2. The flow stress increases as the temperature is lowered and all curves have a tendency to flatten out around a strain of about 0.5. At higher strains the slopes of the stress-strain curves tend to increase as shown by the 175° and 200° curves. The sample pressed at 150°C cracked extensively during hot working which could account for the constant stress exhibited at higher strains.

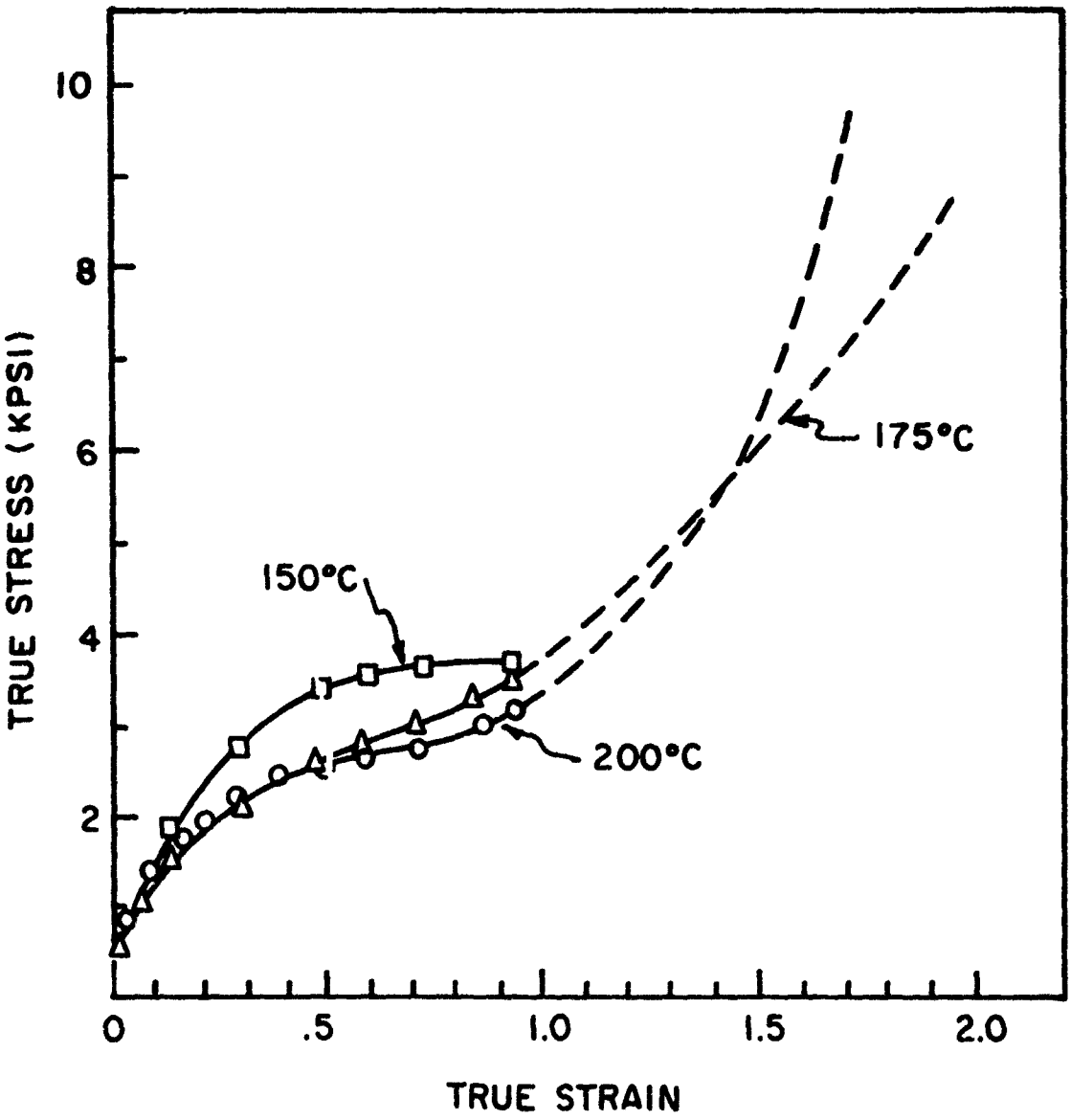

Figure II-2. True stress-true strain curves plotted from data taken during the < 100 > pressing of KCl crystals at a constant ram speed of .012 in/min to 60 percent and 80 percent reduction in thickness at the temperatures shown. The data for strains less than 1.0 were from 60 percent reduction pressings. The dotted lines show typical behavior of 80 percent pressings beyond this point. A curve for 150°C is not shown because pressings at this temperature were usually extensively cracked.

The microstructures of regions taken from near the center of 60 percent pressings made at 150°, 175°, and 200°C are shown in Figure II-3(a), (b), and (c) respectively. These structures are typical of regions throughout the pressings, although fairly extensive deformation banding was observed particularly near the edges of the pressings where flow was greatest. The microstructureof the 150° pressing was extremely difficult to reveal by etch- as evident from Figure II-3 (a). It is not clear, at this time, if the structure is composed of large or small angle boundaries or a combination of both. Fine recrystallized grains are clearly evident in the structures of the 175°C and 200°C pressings. Average grain sizes, as measured from the micrographs by the linear intercept technique, were 5.3 and 5.2 μm for the 175° and 200°C material respectively. (Measurements were not made on the 150°C material.) Grain size differences in adjacent deformation bands were observed to sometimes vary by as much as a factor of 10.

The mechanical properties of the 60 percent pressings, as determined by 3-point bend tests, are listed in Table I-1. The yield stress was taken to be the proportional limit. Also included in the table are the percent reduction, final strain rate, and final forging stress of each pressing. Some single crystal data are included for comparison.

Only one value is given for the 150°C material. The pressing contained many cracks and was in an extremely high state of internal stress. In this state, even gentle sawing on the forging introduced further cracking. The one sample that was tested evidently contained some undetected cracks and failed with no elongation.

The yield and fracture strength measurements on material produced at 175° and 200°C were valid and indicated that these properties do increase with a decrease in working temperature as expected. The yield strengths are in the 4000 to 5000psi range and they represent values seven to ten times those of the single crystals.

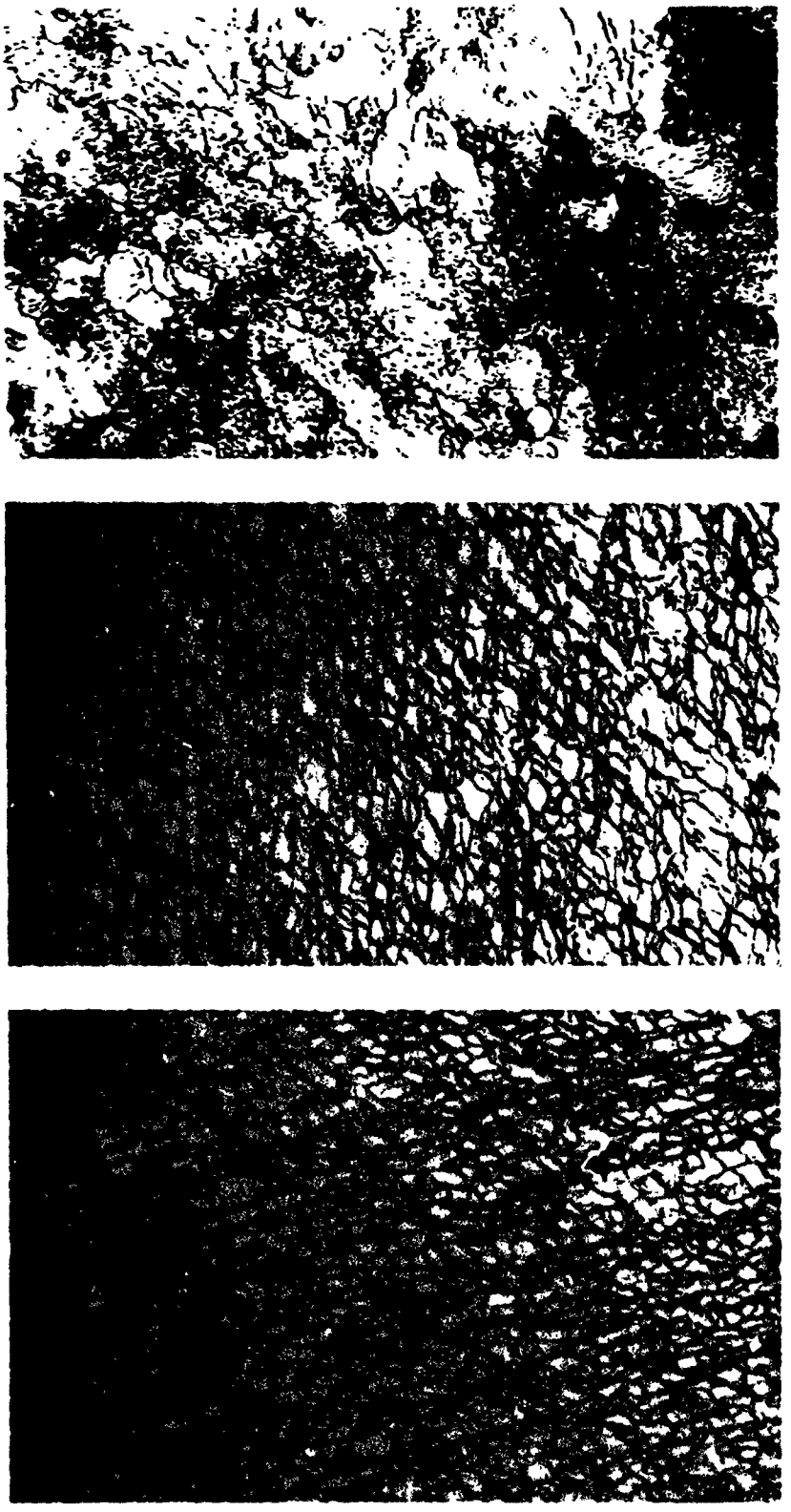

Figure II-3. Micrographs showing the fine grain structure of 60 percent pressings made at (a) 150°C, (b) 175°C, (c) 200°C. Magnification 400X. Nominal grain sizes are indicated on the figure. The pressing direction was along the short side of the micrographs.

Table I-1. Mechanical Properties (3-point bend) and forging data of 60 percent KCl pressings.

Pressing Number	Temp (°C)	Percent Reduction	Final Strain Rate (min^{-1})	Final Forging Stress (psi)	Yield Stress (psi)	Fracture Stress
41	150	60	.019	3700	~2500	~2500
40	175	60	.019	3800	5307	8684
					4246	8138
					4033	8765
38	200	61	.020	3300	4546	7009
					4506	7117
					4089	5174
KCl crystal with <100> parallel to beam axis.					577	1634
					527	1563
					475	1629

Although the pressing made at 150°C contained arrays of cracks, it was intact and could be sectioned for determination of its texture. The (100) and (110) pole figures from the 150°C pressing are shown in Figures II-4 and II-5 respectively. The texture is neither (100) or (110). Allowing for the spread in the orientations, the texture can be approximated by (113). The (100) and (110) pole figures from a 60 percent pressing made at 175°C are shown in Figures II-6 and II-7 respectively. The pole figures shown in Figures II-6 and II-7 indicate again that the compression axis lies in the vicinity of (113) or (112) on the great circle between (001) and (111).

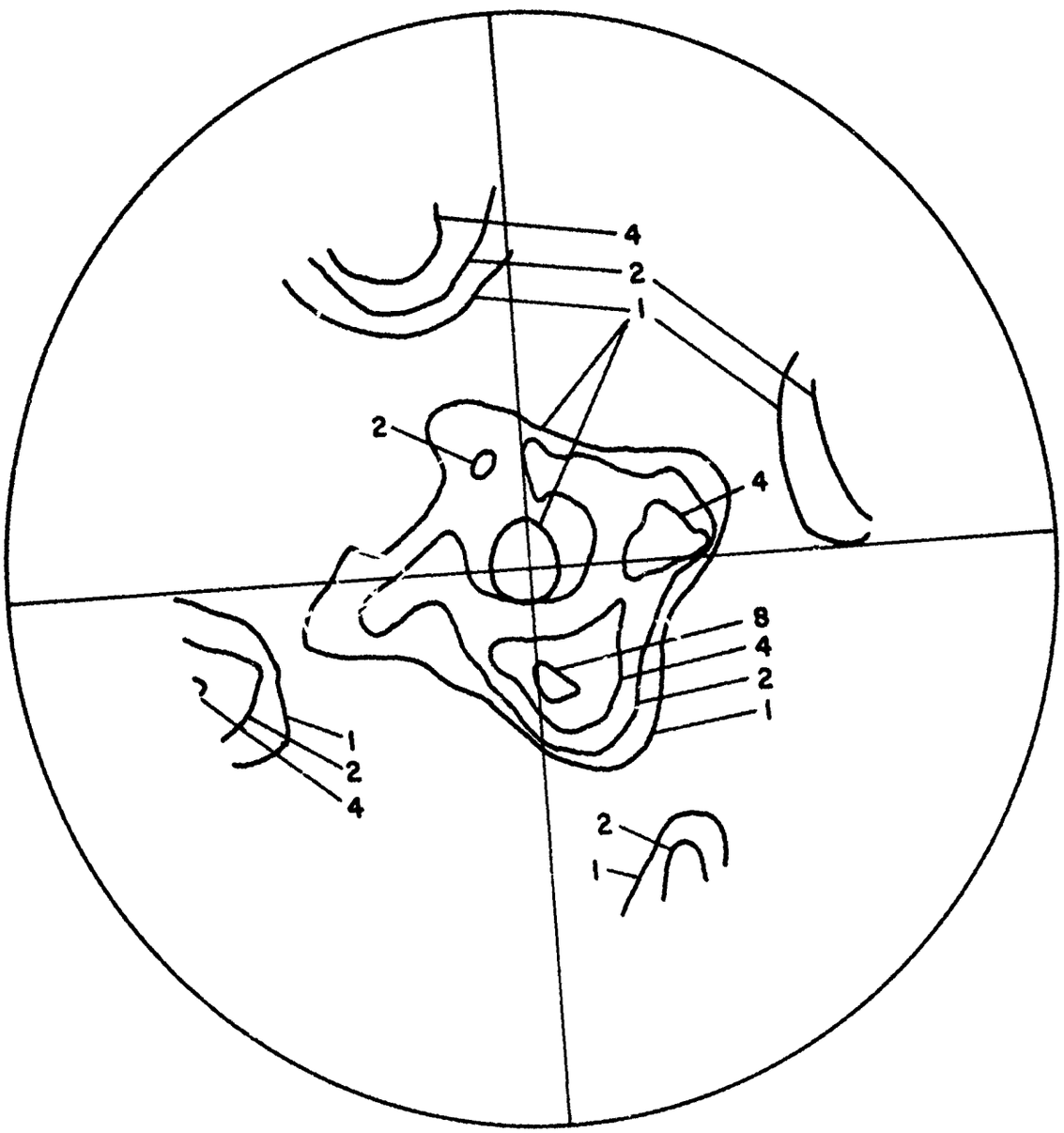

Figure II-4. (100) pole figure from a 60 percent pressing made at 150°C. The numbers indicate arbitrary intensities.

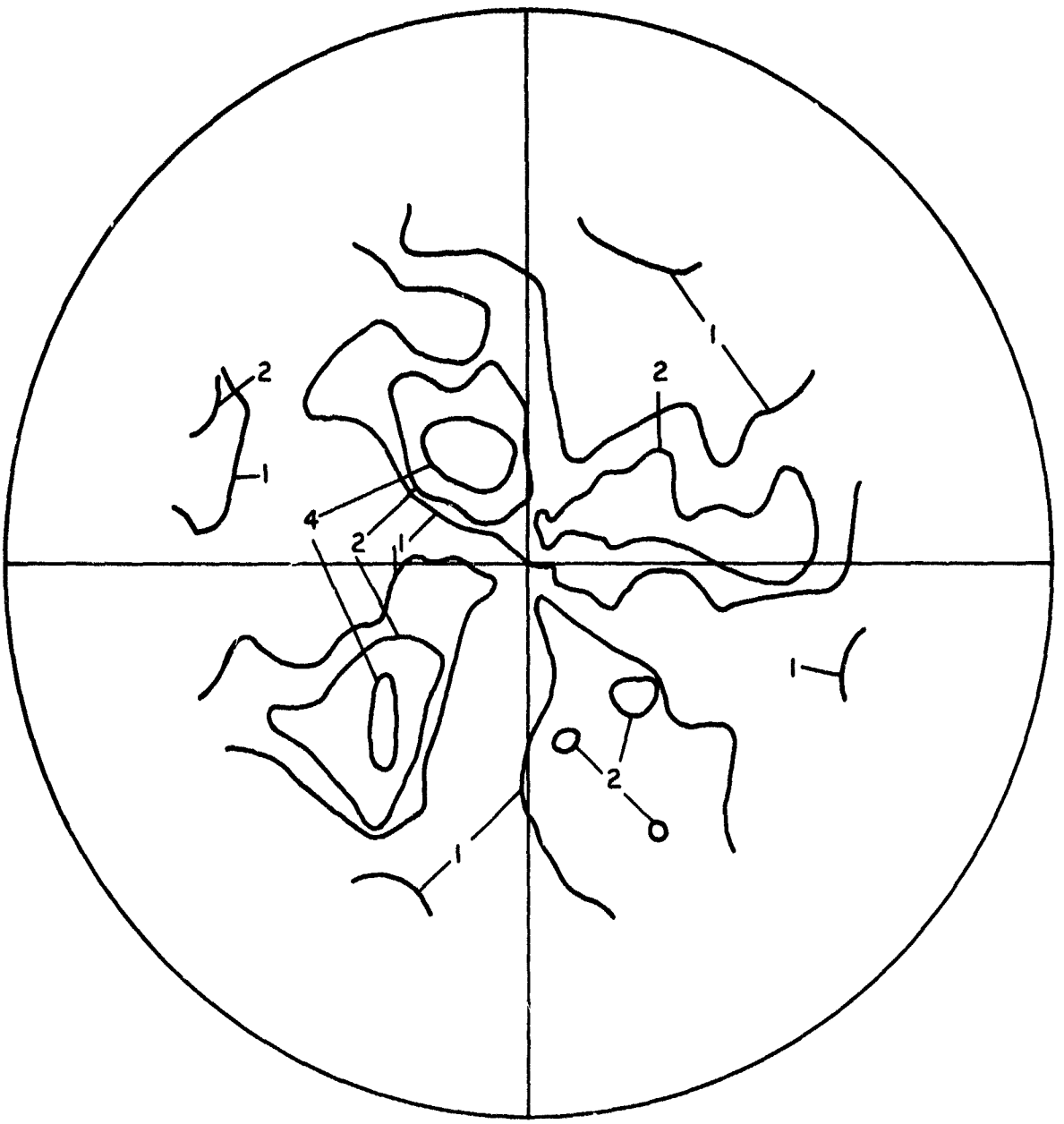

Figure II-5. (110) pole figure from a 60 percent pressing made at 150°C. The numbers indicate arbitrary intensities.

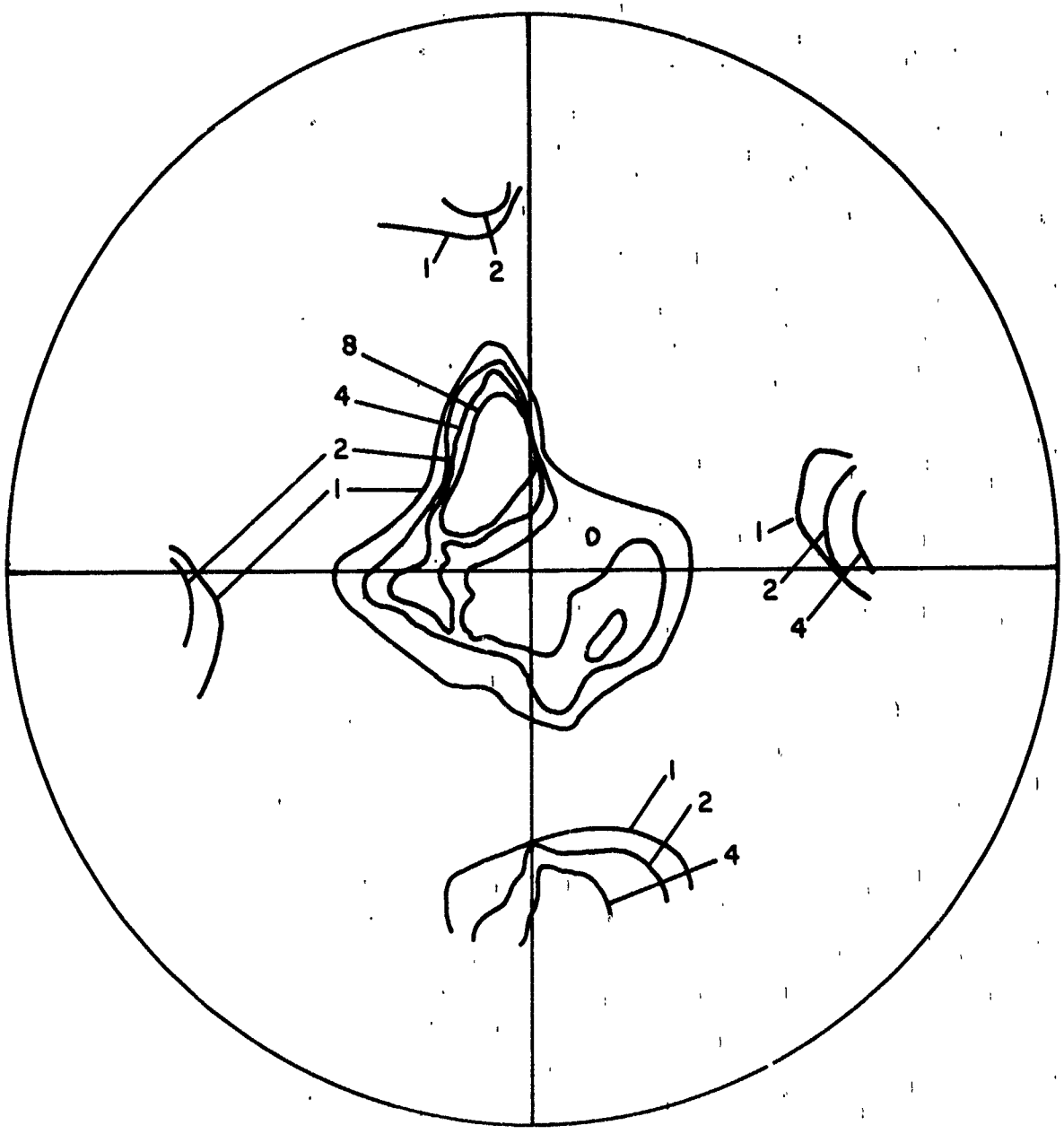

Figure II-6. (100) pole figure from a 60 percent pressing made at 175°C. The numbers indicate arbitrary intensities.

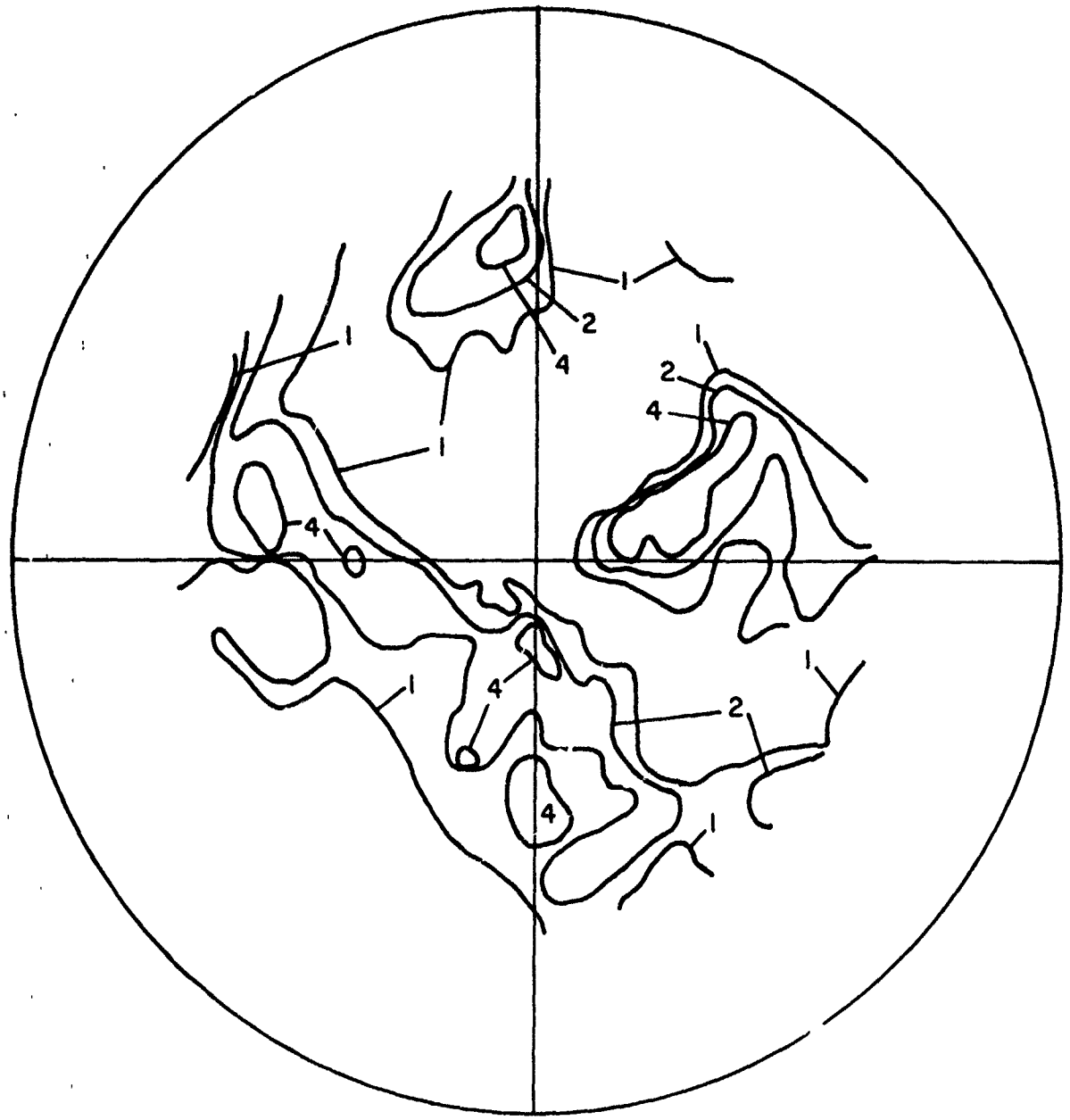

Figure II-7. (110) pole figure from a 60 percent pressing made at 175°C. The numbers indicate arbitrary intensities.

The (100) and (110) pole figures from a 60 percent pressing made at 200°C, shown in Figures II-8 and II-9, also yield a texture close to those mentioned above. The point to be made is that 60 percent pressings do have a compression texture and the texture is fairly sharp. This texture is not (100) or (110) and can be more closely approximated as lying somewhere in between.

b. Crystals Pressed to 80 Percent Reduction -- True stress-true strain curves obtained on pressings carried out to 80 percent exhibited behavior such as that shown by the dotted curves of Figure II-2. A curve at 150°C is not shown because these samples fractured extensively during pressing. As true strains of 0.5 are exceeded the flow stresses were observed to increase steadily with reduction till values of 8 to 10 kpsi were finally reached by the end of the pressing. We observed no systematic decrease of the finishing stress level with increase in temperature in samples pressed at 175° and 200°C as indicated on Figure II- 2.

Micrographs illustrating the fine grain structure resulting from the 80 percent pressing are shown in Figure II-10 (a), (b), and (c) for pressings made at 150°, 175° and 200°C respectively. These micrographs were taken from regions near the center of the pressing. Extensive banding was observed in these pressings as well as in the 60 percent pressings and, again, the grain size was observed to vary from band to band. Average grain sizes measured by the linear intercept method on the micrographs shown in Figure II-10 are 3.9, 3.7, and 4.2 μm for material pressed at 150°, 175°, and 200°C respectively.

Some interesting behavior was observed in the 80 percent pressings which prevented valid mechanical property determinations to be made on the 150° and 175°C material. This behavior will be briefly mentioned at this time and discussed in more detail in the next section of this report. It was a surprise to discover that all of the samples pressed to 80 percent reduction in

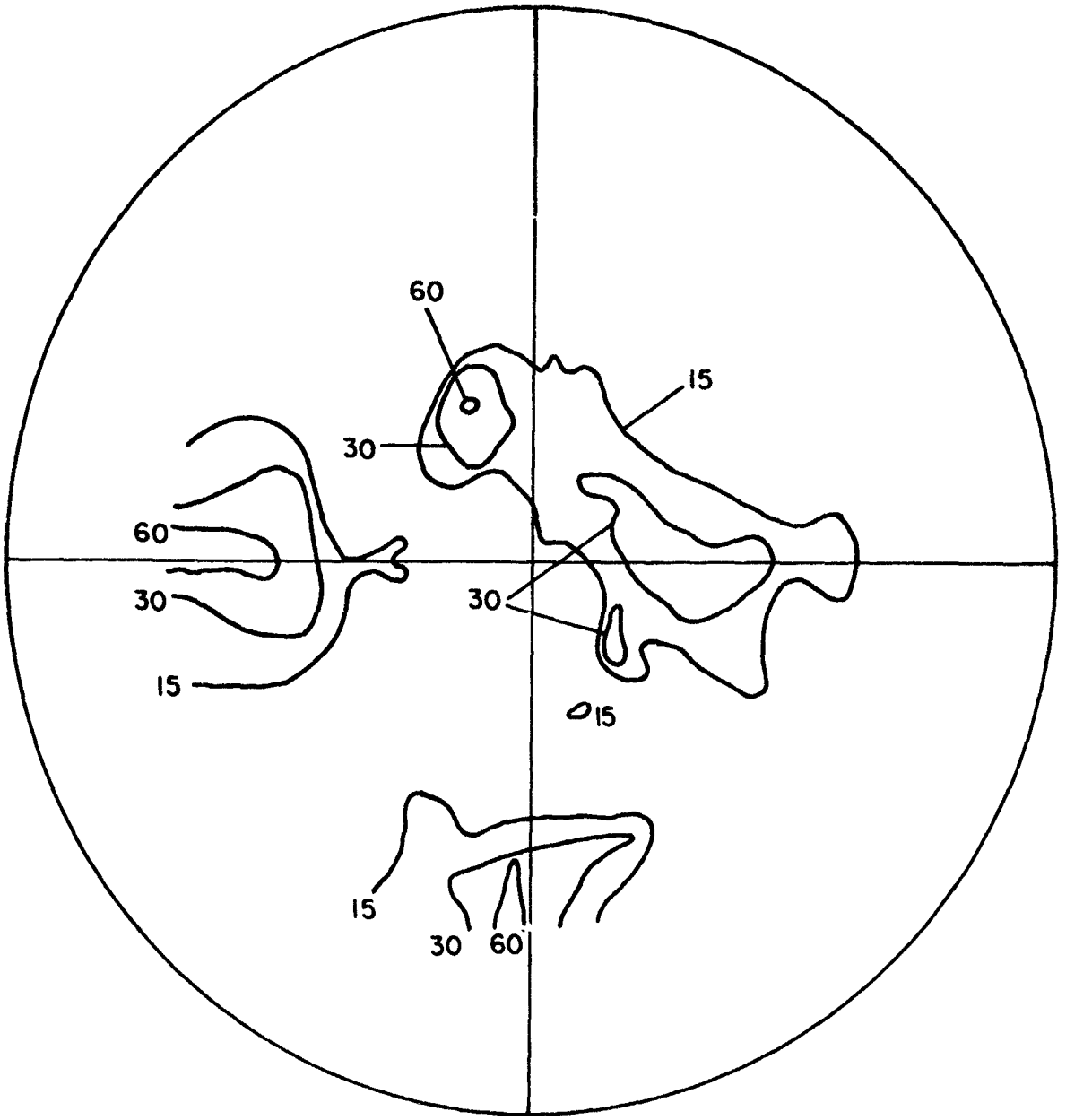

Figure II-8. (100) pole figure from a 60 percent pressing made at 200°C. The numbers indicate arbitrary intensities.

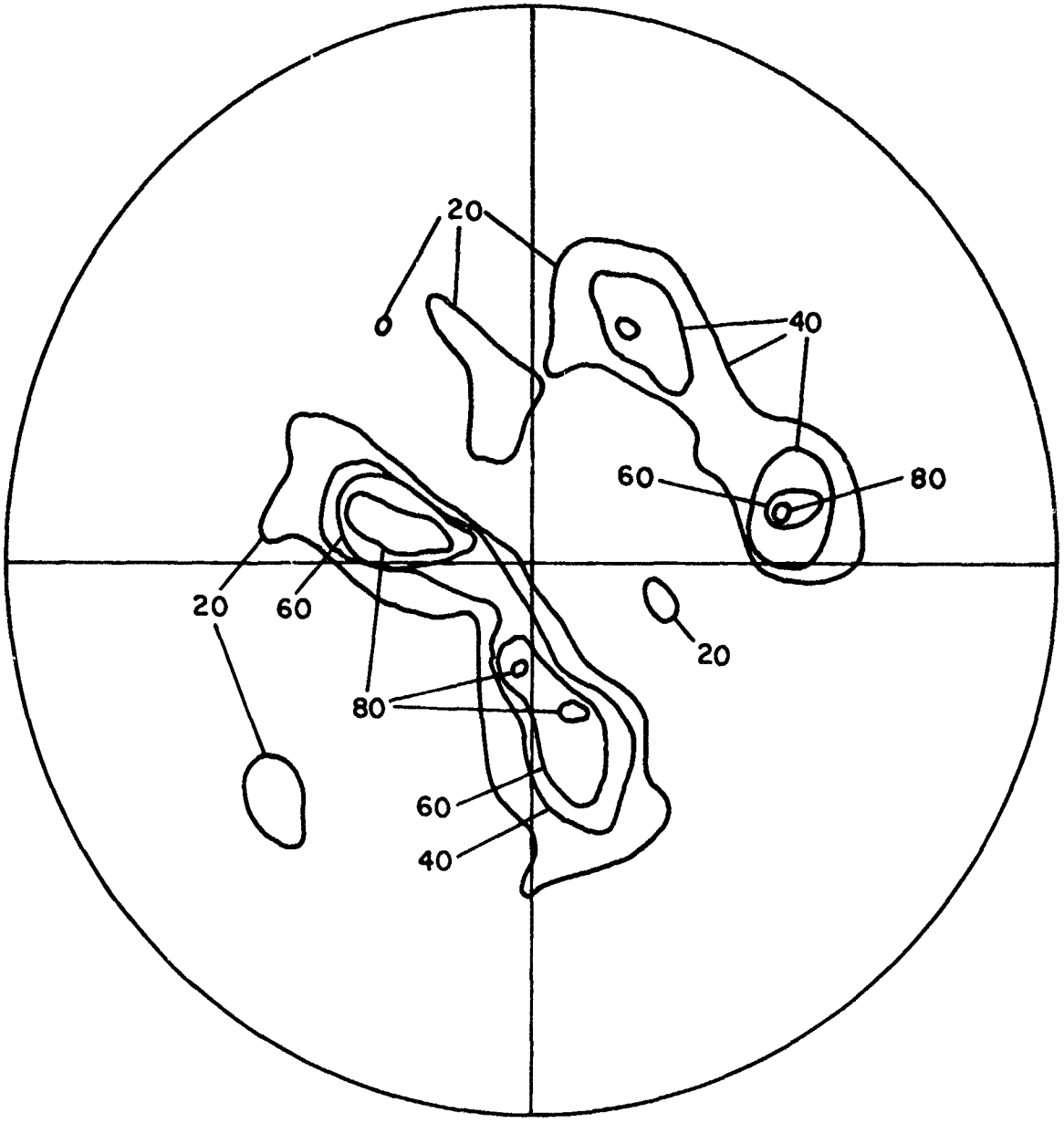

Figure II-9. (110) pole figure from a 60 percent pressing made at 200°C. The numbers indicate arbitrary intensities.

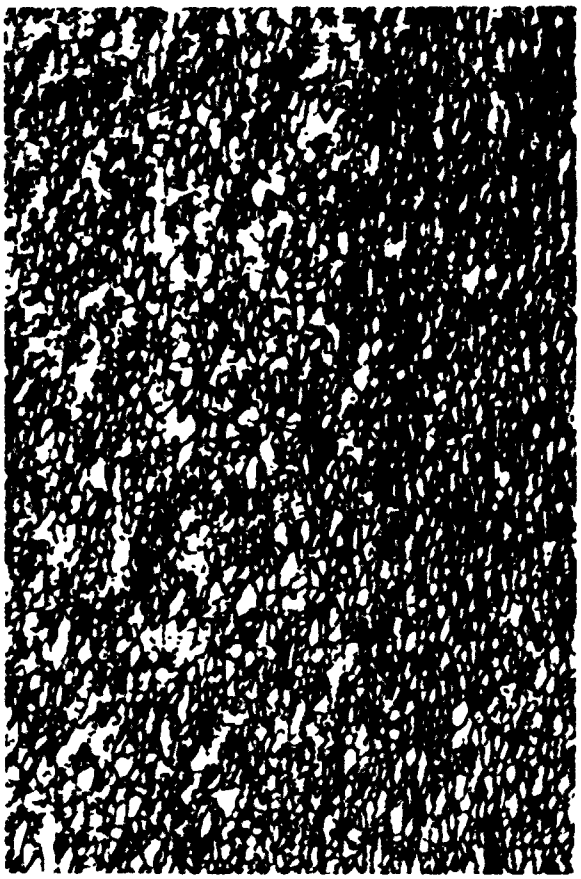

(a) 3.9μm

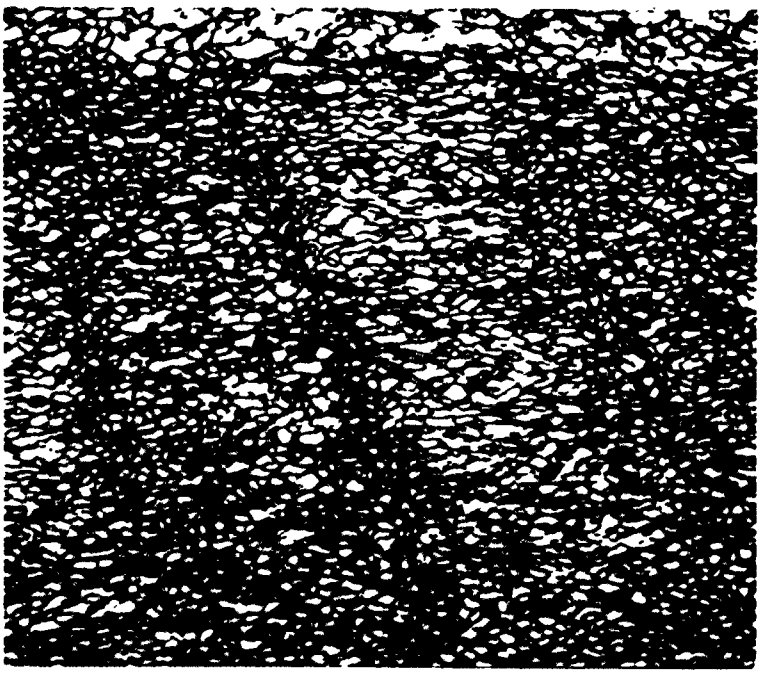

(b) 3.7μm

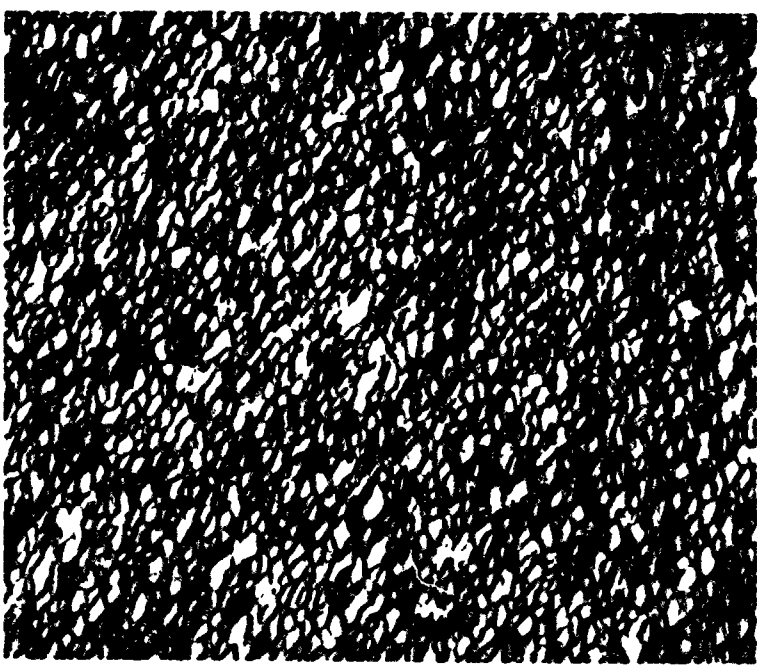

(c) 4.2μm

Figure II-10. Micrographs showing the fine grain structure of 80 percent pressings made at (a) 150°C, (b) 175°C, (c) 200°C. Magnification 400X. Nominal grain sizes are indicated on the figure. The pressing direction was along the short side of the micrographs.

thickness were unstable and underwent extensive secondary recrystallization at room temperature. The secondary grains were typically quite large and, as will be shown later, propagated at an alarming rate through the fine grained matrix. An example of this behavior is shown in Figure II-11 for a pressing made at 175°C. The large grains seen in the figure were growing in from the top surface of the pressing. A large portion of the boundaries of these secondary grains were observed to be straight, indicating certain crystallographic boundaries to be quite stable during secondary recrystallization. Most likely these are $\{100\}$ or $\{110\}$ as suggested by the large grain shown in Figure II-12 from an 80 percent pressing made at 200°C. We have some evidence to indicate that the stability of these straight boundaries increases with decreasing working temperature. Bend test data taken on samples cut from 80 percent pressings made at 200°C are listed in Table II-2 along with pressing data taken at all three temperatures. The low and scattered values of the yield and fracture strengths were attributed to the fact that room temperature secondary recrystallization had commenced in these samples before testing. Bend tests on material pressed to 80 percent reduction at 150° and 175°C were not made since the samples already contained extensive regions of large grains by the time they were to be sectioned into beams for testing.

Since the structures were unstable only pole figures made immediately following pressing were valid. The (110) pole figure of an 80 percent pressing made at 200°C is shown in Figure II-13. In contrast to the 60 percent pressing results, the texture of the 80 percent pressing is clearly (110). A (110) pole figure taken on the same sample 24 hours later indicated large recrystallized grains to be forming with their $\{110\}$ poles about midway between the central $\{110\}$ pole and those away from the center. These are shown as crosses on Figure II-13.

Figure II-11. Micrograph showing large grains resulting from room temperature secondary recrystallization of an 80 percent pressing made at 175°C. The large grains are growing into the fine grained matrix from an outside surface of the pressing. The pressing direction is along the short side of the micrograph and the outside surface of the pressing is close to the top of the micrograph. Magnification 100X.

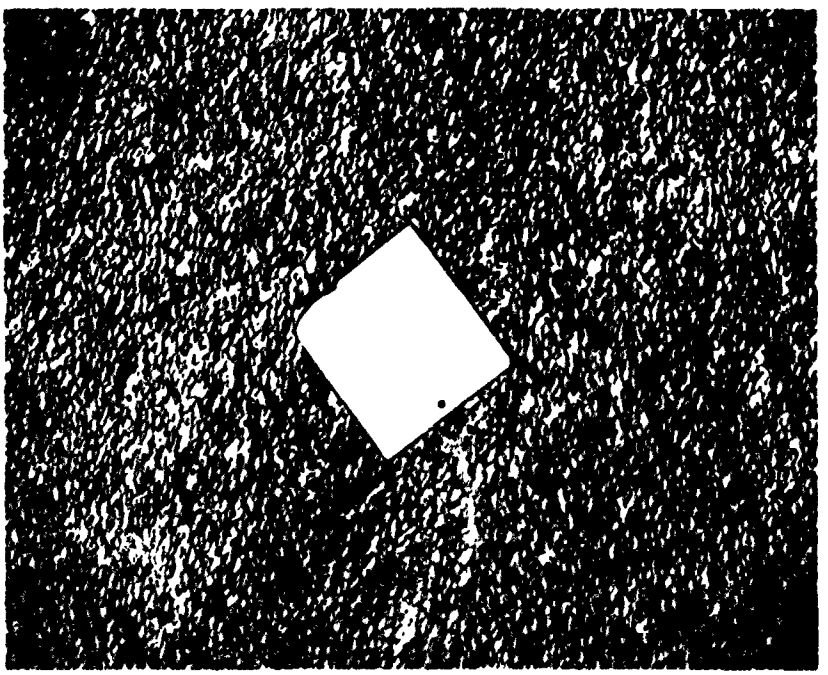

Figure II-12. Isolated grain resulting from room temperature secondary recrystallization of fine grained matrix in an 80 percent pressing made at 200°C. The pressing direction is along the short side of the micrograph. Magnification 200X.

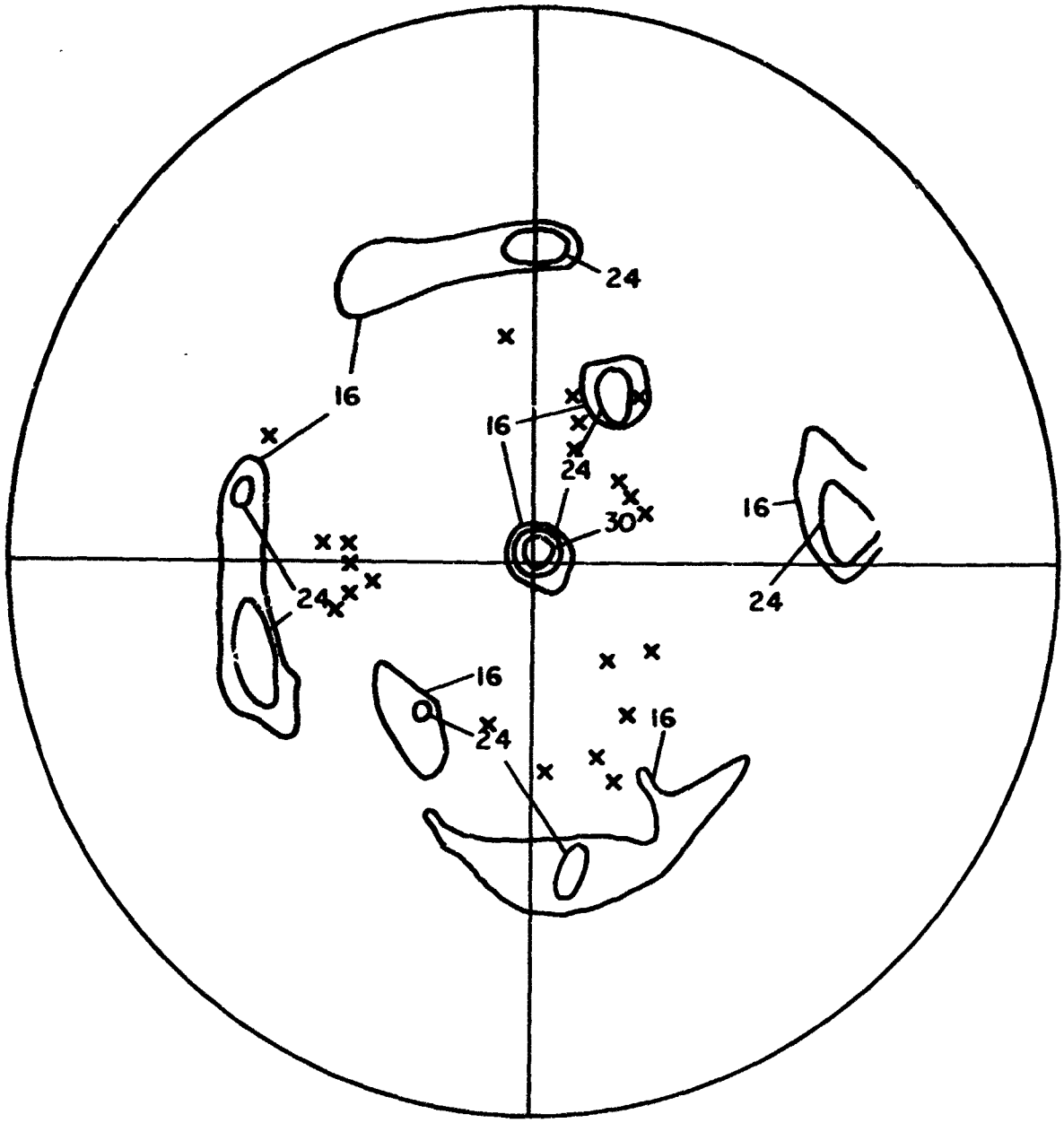

Figure II-13. (110) pole figure from an 80 percent pressing made at 200°C. The crosses indicate the positions of large individual grains that formed in the fine grained matrix during 24 hours at room temperature. The numbers indicate arbitrary intensities.

Table II-2. Mechanical properties (3-point bend) and forging data taken on 80 percent pressings.

Pressing Number	Temp (°C)	Percent Reduction	Final Strain Rate (min^{-1})	Final Forging Stress (psi)	Yield Stress (psi)	Fracture Stress
36	150	84	.049	~8000	*	-
35	175	81	.040	10,000	*	-
34	200	82	.042	9600	592	676
					1987	2897
					1347	2105
37	200	80	.038	8500	2836	5139

*Data not taken due to extensive secondary recrystallization of material.

c. Grain Boundary Mobility Measurements on Unstable 80 Percent Pressings -- As mentioned above, we noted that the 80 percent pressings were undergoing rapid structural changes (secondary recrystallization) at room temperature. It was further noted that many of the boundaries of the secondaries were quite straight and appeared to exhibit crystallographic relationships with each other (see Figures II-11 and II-12.)

We have, at this time, made some preliminary observations concerning secondary recrystallization in the unstable 80 percent pressings, these are reported below. In a typical experiment a sample was polished and etched and a region of the sample containing large secondaries with straight boundaries was photographed. The sample was then kept at room temperature, or 50° or 70° for a certain period of time after which the surface was lightly re-etched and the same region photographed. Since the etching procedure removed very little material it was possible to obtain records of the boundary

movements at the three temperatures as a function of time. The following points were noted

1. The straight boundaries remained straight and always moved parallel to themselves at rates that did not vary with time.

2. The fastest boundaries were always the straight boundaries.

3. In the samples examined (one at each temperature) different boundaries moved at different rates. This does not, however, discount the presence of a certain intrinsic rate of motion of a particular type of boundary (e. g., $\{100\}$ or $\{110\}$) in a particular structure for the angle of incidence the boundaries made with the surface could not be determined. It was noted, however, that supposedly $\{100\}$ or $\{110\}$ boundaries lying normal to the surface (e. g., as in Figure II-12) appeared to move at the slowest rates.

The results of the measurements of the rates of straight boundary migration made to date are presented in Figure II-14. These data were all taken on samples cut from an 80 percent pressing made at 200°C. The initial structure of the material is that shown in Figure II-10 (c) with an average grain size of about 5 μm.

A number of comments can be made concerning Figure II-14. Note first that the rate of migration of the boundaries of the large grains growing into the structure were significant and measurable even at room temperature. The rates increased by two orders of magnitude when annealing was carried out at 50°C, but then dropped at the higher annealing temperature of 70°C. This is taken to indicate that the driving force for secondary recrystallization in this material depends on stress as well as temperature and that the drop in boundary migration rate at the higher temperatures is a result of recovery processes decreasing the internal stress in the material. This clearly

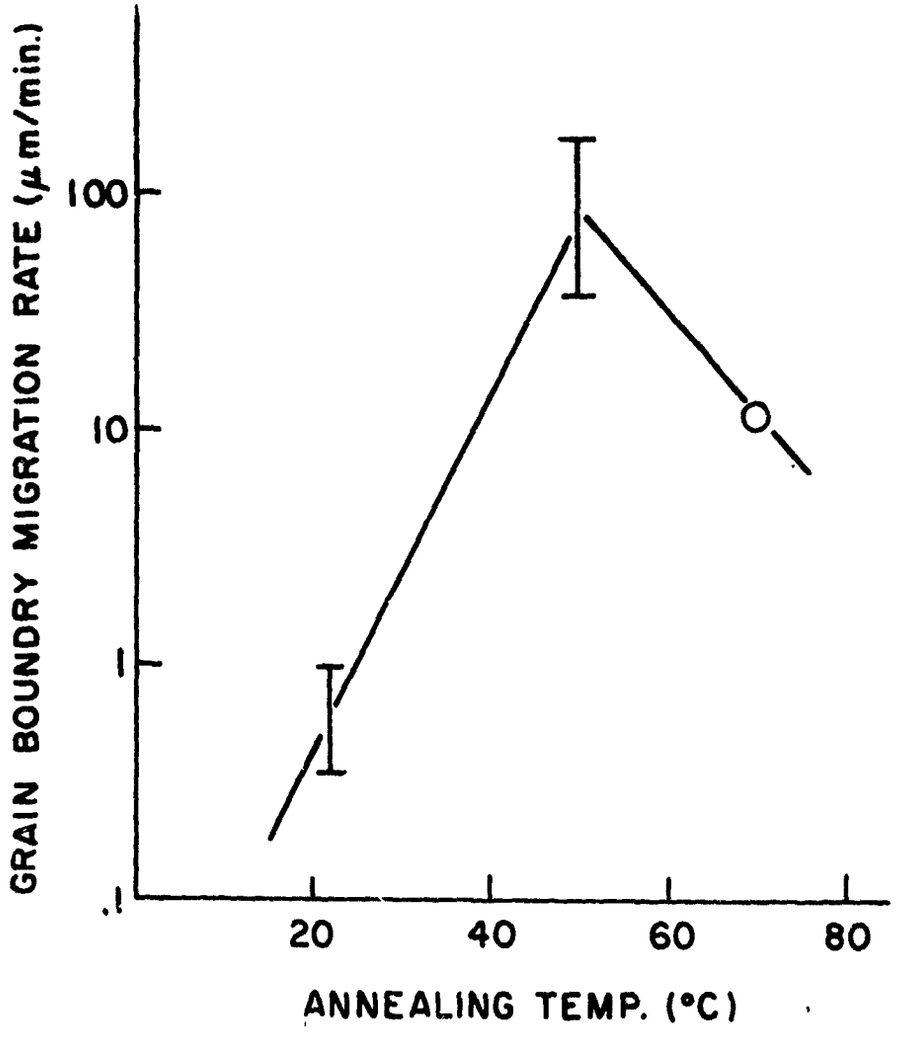

Figure II-14. Rates of migration of straight boundaries of grains resulting from the secondary recrystallization of an 80 percent pressing made at 200°C. The rates were determined at room temperature, 50°C and 70°C. The bars indicate the range of values observed for a number of different boundaries at each temperature.

points to the advisability of using stress relief anneals to stabilize the as-formed microstructures (and mechanical properties) of these materials.

B. ROLLING

The following paragraphs describe our efforts to date to produce polycrystalline halides by hot rolling single crystal KCl billets. Hot rolling is being investigated as a means of producing polycrystalline material for a number of reasons:

1. The deformation during hot rolling is much more localized than in press forging and the resulting structures should reflect this.

2. Hot rolling imparts directional properties to the material. The amount of directionality can be controlled by cross rolling.

3. Both rolling and press forging can be used sequentially on the same billet to alter the structure and properties of the material.

4. Since the contact area is small, the loads during hot working are low and lubrication might not be a critical problem.

At this time most of our efforts have been concerned with preparation of the equipment which is now operational and is described below.

During this study we used a Stanat Model TA315 two-high mill mounted with 5-inch dia. x 8-inch wide rolls. To process halides we made three modifications to the mill. First, we installed internally heated rolls capable of running at temperatures up to 370°C. Second, we installed fore and aft tunnel heaters on the mill for pre and post heating of the billet during a hot rolling operation. Finally, we modified the drive to the rolls to enable us to

vary the roll speed to produce deformation rates in the billet commensurate with those found to be successful during our press forging study. By installing two gear boxes on the mill we can now continuously vary the roll speed from 0.012 revolution/min. to 1.0 revolution/min.

SECTION III

OPTICAL PROPERTIES

The experimental techniques used to evaluate the polycrystalline halides and some preliminary observations and deductions based on our experiments are discussed in this section. The two main techniques used for evaluating the optical behavior of halides are calorimetry and holographic interferometry (discussed below). Also presented are calculations of the temperature distribution to be expected from laser irradiation and the optical and thermodynamic properties of the halide.

A. CALORIMETRY

The basic calorimetric technique used in our measurements is that described by Horrigan and collaborators[9]. The actual evaluation of the absorbed power is made using the slope technique as described by Skolnik[10]. Figure III-1 shows the schematic diagram of the calorimetric measuring equipment. The sample is held by four Delrin cylinders, 1/4 inch in diameter x 3/4 inch long, that are attached to a modified Lansing gimbal mount. The cylinders have a very small contact area with the sample and have low thermal conductivity. By using four cylinders spaced 90 degrees apart, both round and square samples can be held in the same holder. A differential thermocouple made from 2 copper and 1 constantan lengths of wire is used to measure the temperature difference between the aluminum frame of the gimbal mount and the sample during irradiation. One of the thermocouple junctions is attached to the gimbal mount while the other one is attached with Teflon tape to one of the Delrin cylinders. The cylinder is then pressed tightly against the halide sample. The copper leads from the differential thermocouple are soldered to copper clip-leads that are used for connections to instrumentation. The two independent adjustments on the gimbal mount allow us to orient the sample so as to prevent unwanted reflections of the CO_2 laser beam.

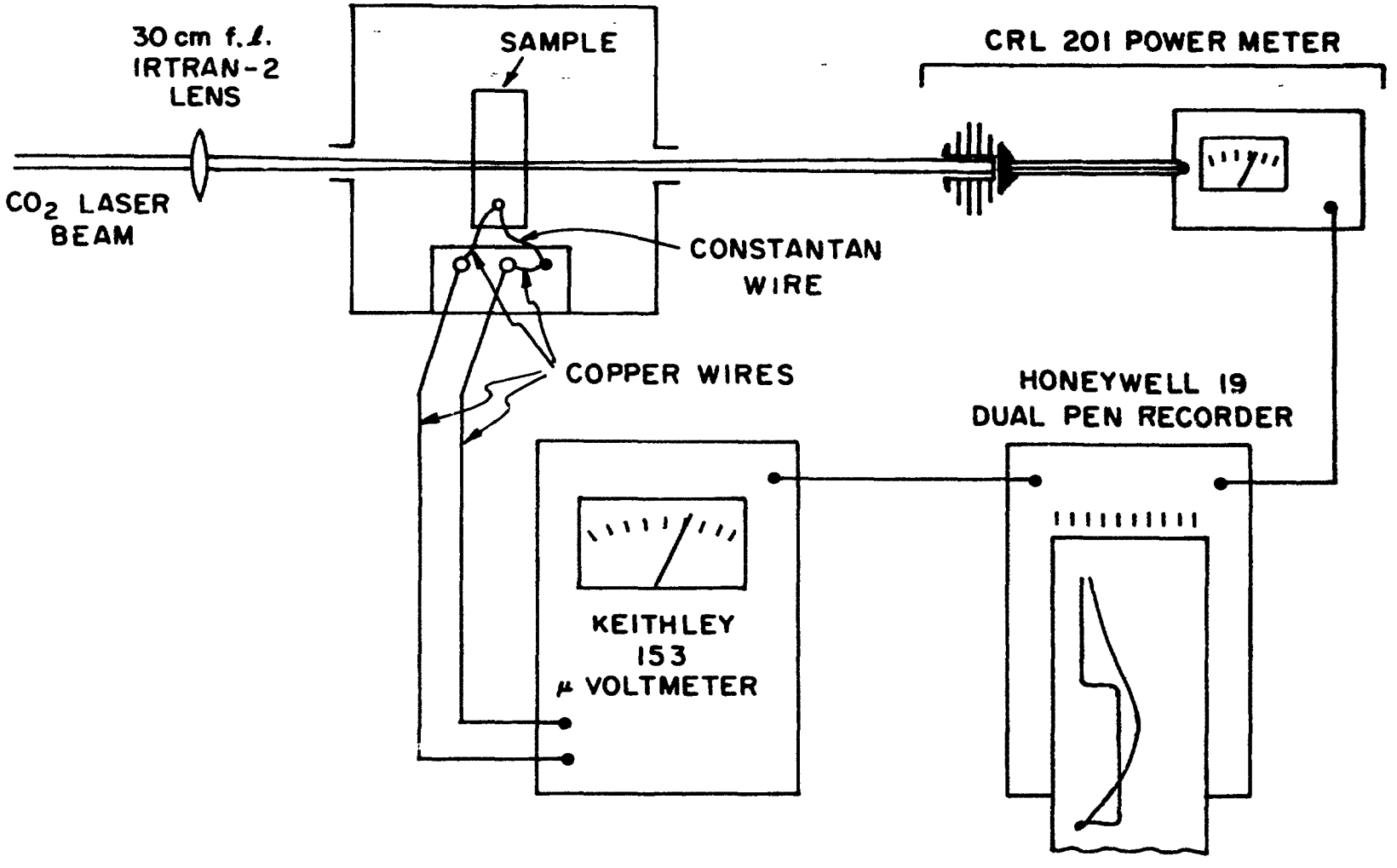

Figure III-1. Calorimetric apparatus for measuring absorption coefficient of halides.

The assembly for holding the samples, with a sample in place, is shown in Figure III-2. The sample holder is placed inside a brass cylinder that can be evacuated and which has three ports. The inside of the drum is spray-painted with 3M Nextel black velvet paint. One of the ports carries the leads from the microvoltmeter and the other two, which are in line, transmit the CO_2 laser beam into and out of the drum. The container can be evacuated by putting windows in the ports. However, early experiments indicated that the results obtained in the calorimeter were the same whether it was operated in a vacuum or air filled. Thus, all measurements made since the early part of this program have been made in air. The main function of the container appears to be the reduction of drafts and the provision of a stable temperature environment in which to make the measurements.

The CO_2 laser beam is focused onto the sample using a 30cm focal length lens made of Irtran-2. After passing through the sample the beam diverges and is intercepted by a Coherent Radiation Laboratories Model 201 power meter. The output of the power meter is recorded on one channel of a dual pen Honeywell Model 19 strip chart recorder. The output of the differential thermocouple is sent into a Keithley Model 153 microvoltmeter whose output is recorded by the second pen of the strip recorder. In this manner a synchronized record of the instantaneous power and temperature rise during the heating-cooling cycle is obtained. A typical example of this record is shown in Figure III-3 in which a single crystal sample of potassium chloride (#C10) from Optovac, cleaved one day prior to the measurement, was irradiated with a transmitted power of 18 watts. The sample dimensions were 2.27 x 2.52 x 1.45cm. The laser beam transversed the smallest dimension. From Figure III-3 and using values of the density, heat capacity and refractive index for potassium chloride given in the AIP Handbook[11] we obtained an average value of the absorption coefficient of the sample of $\beta = (9.3 \pm .9) \times 10^{-4}$ cm^{-1}. This average value is obtained from the sum of the slopes at three different points in the heating and cooling cycle. The results obtained from the data of Figure III-3 can be used as the base value

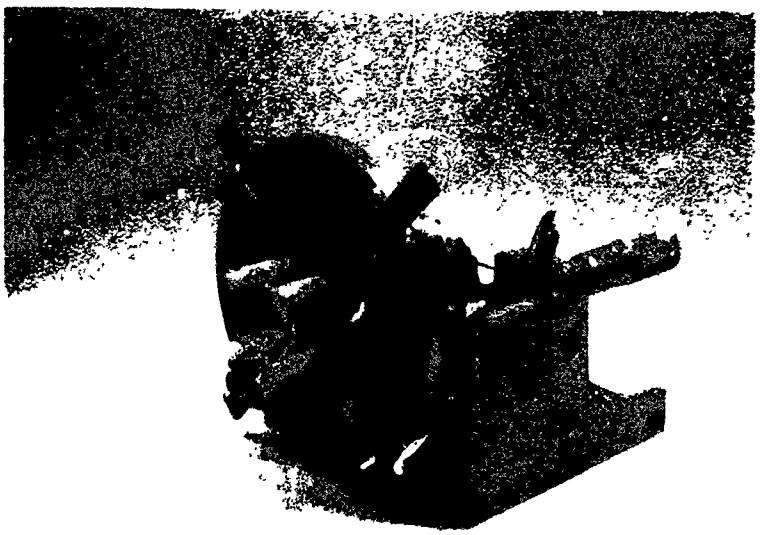

Figure III-2. Sample holder used for calorimetric and interferometric measurements.

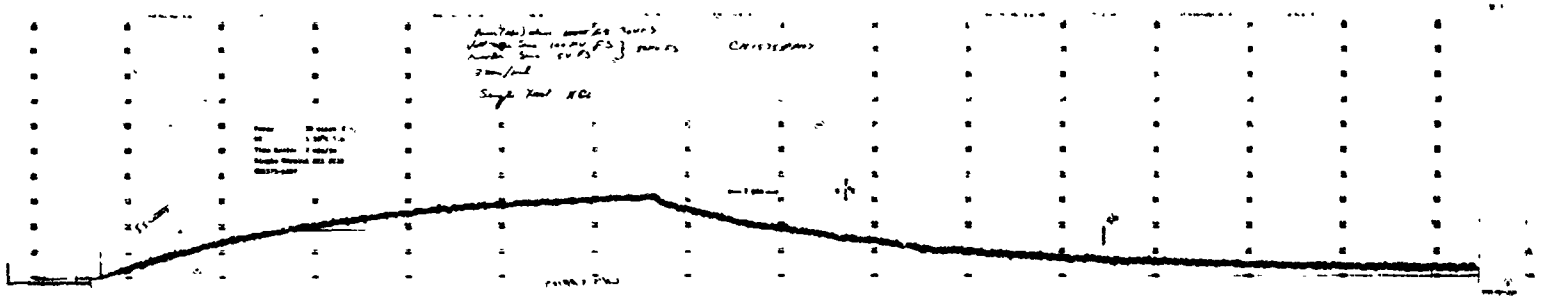

Figure III-3. Calorimeter trace for cleaved single crystal of potassium chloride (#C 10)

to judge the effect of processing on the optical loss in the polycrystalline halides.

Measured absorption coefficients in the polycrystalline halides range from a few times the value for the single crystals to as high as 20 times larger. The results obtained appear to be limited by the surface preparation of the polycrystalline material instead of the processing parameters used in producing it. This, of course, assumes that one is measuring material that is free from cracks or any obviously strong scattering centers, which is the case with most of the samples prepared by the hot working techniques used in our laboratory. It is clear, therefore, that the validity of the comparison of absorption coefficients in the polycrystalline material to that of the starting single crystal will require the development of polishing methods capable of producing surfaces of comparable quality in the single crystal and polycrystalline material. Until that goal is achieved, the main value of the calorimetric measurements will be in providing a method of comparing polycrystalline material prepared under varying processing parameters.

B. HOLOGRAPHIC INTERFEROMETRY

In a program aimed at producing a material capable of handling the flux densities produced by a high power laser, it is desirable to measure both the absolute optical homogeneity of the window in a passive state, as well as the effect of irradiation or stress on the optical homogeneity of the window material. The desirability of measuring optical homogeneity under dynamic conditions has been well established in the case of pulse ruby lasers.

We have known from the start of this program that the production of high quality optical surfaces on halide materials is a major problem. Because of this understanding we have tried to identify methods of evaluation that would allow us to proceed with tests without depending on having a high

quality optical surface. For the absolute measurements of optical homogeneity we have chosen to look at the stress induced birefringence and scattering, and for the effects of irradiation and stress on the optical homogeneity we are attempting to use the technique of holographic interferometry. The following paragraphs discuss our attempts to use the latter to evaluate changes in the optical path produced by irradiation with a CO_2 laser. Our attempts to date have had limited success because of a number of experimental difficulties, but the ability of the technique to show quantitative changes in optical path has been established and will be discussed below.

Holographic interferometry is considerably more complicated than conventional Twyman-Green interferometry, but it offers some unique advantages since it is a truly differential method. For conventional interferometry, a transparent object whose optical homogeneity is to be evaluated is compared to an essentially perfectly homogeneous medium. This means that the interferogram obtained in a Twyman-Green interferometer contains information about the surface condition as well as the bulk index of refraction homogeneity. Thus, measurements of laser-induced changes in optical thickness require surfaces that are at least flat to a fraction of a wavelength and preferably parallel to a few seconds of arc. For studies of index homogeneity or stress-induced effects it should be possible to immerse the sample in an index-matching fluid that does not dissolve the halide, thereby avoiding the need for preparing surfaces of optical quality to perform interferometric measurements. In the case of laser induced changes in the optical thickness of the sample it is not possible to use a fluid because the thermal effects produced by the beam in the fluid are dominant. In holographic interferometry one compares the optical path through the sample at the time that the hologram is made to the optical path at a later time after changes have been made in the sample. As an example, one can make a hologram of a polycrystalline halide sample which is not of uniform thickness and that has scratches on the surface and compare the optical thickness point by point with the optical thickness during irradiation of that sample with the beam from a carbon

dioxide laser. Thus, in the absence of techniques for producing optical-quality surfaces in these materials this technique allows one to evaluate changes in samples with very imperfect surfaces.

The holographic interferometer used in this work is shown in Figure III-4. The light source is a Spectra Physics Model 120 helium-neon laser that operates in three longitudinal modes and has a coherence length of approximately 5cm. This means that one can have an optical path difference of approximately 5cm between the two paths of the interferometer without losing any sizable fraction of the information contained in the interferogram. The beam from the laser is divided into two beams by a dielectric-coated beam splitter and each beam is sent through an expanding telescope and a spatial filter. The telescopes have an expansion factor of approximately 20X and the spatial filters are pinholes of 10μm diameter. The reference beam, which is made to diverge slightly after going through the expanding telescope, goes directly to the holographic recording medium. The object beam is allowed to impinge on a diffuser plate after exiting from the expanding telescope. The diffuser is a Kodak ground glass plate which has a mean particle size of approximately 5μm. After being diffused the light is transmitted through the sample and goes to the holographic recording medium where it interferes with the reference beam to form a Fresnel hologram. In this arrangement what is actually recorded is a hologram of the diffuser plate as seen through the halide sample. The reason for using a diffuser is that it produces, in effect, a very large number of point sources which are used to illuminate the halide sample, thus allowing for a multiplicity of paths between any point in the halide and the recording medium. This in turn allows one to image the sample for later viewing. If a diffuser were not used, the field of view as seen from any finite aperture looking at the holographic reconstruction would be determined strictly by the divergence of the beam exiting from the expanding telescope. This kind of illumination essentially produces a shadowgraph of the object which prevents one from seeing a true image[12].

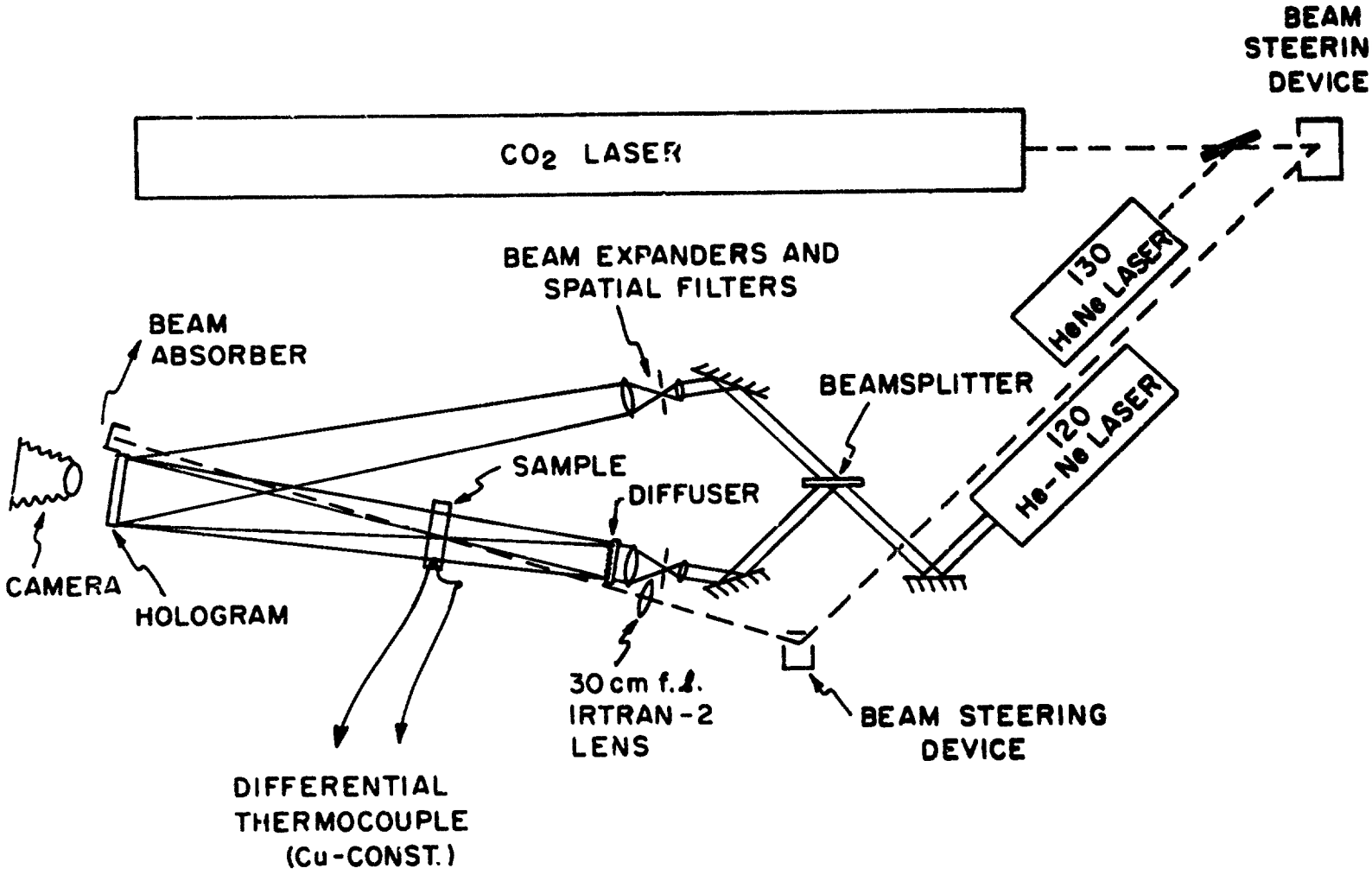

Figure III-4. Holographic interferometer used in measuring changes in optical thickness of transparent material produced by CO_2 laser irradiation or externally applied stress.

Using a diffuser does introduce a complication into the photographing of interferograms. This is the problem of speckle or spatial noise in the film plane. The speckle is a result of the finite size of the particles in the diffuser and it becomes more noticeable as the aperture through which the object is viewed is decreased[13].

In all the holographic work performed in the current quarter the recording medium has been 4 x 5 inch Kodak 649F glass plates. The plate is placed in a gimbaled holder where the hologram is recorded. It is then removed and developed, using the procedure described in Reference 13, to minimize the dimensional changes in the emulsion which cause unfaithful reproduction of the object wave on reconstruction. When the hologram is illuminated by the reference beam it reconstructs the wavefront characteristic of the object in the undeformed state. This wavefront is then made to interfere with the wavefront generating from the object which is being simultaneously illuminated. In the absence of object deformation, and if the film can be replaced in the exact position where the hologram was recorded, one is able to completely extinguish the object in the region of interference. Then, if the object begins to deform, interference fringes can be seen to appear corresponding to half wavelengths of deformation per fringe. However, if the film is not replaced in exactly the same position that it was during recording of the hologram, the plane where the fringe visibility is optimum does not coincide with the plane of the object and can, in fact, be a considerable distance from the object. Then, to relate the fringe pattern to spatial temperature distribution it is necessary to photograph the fringe pattern using a very large F number in the camera lens (this means a very small aperture, typically F/36). This has been our experience to date with the photographic film and we have typically had to photograph the fringe pattern with F stops ranging from 25 to 36.

C. INTERFEROMETRIC RESULTS

Thus far all attempts to obtain interference fringes caused by heating of polycrystalline halides with the beam from a carbon dioxide laser up to flux densities of approximately 5000 watts/cm^2 have failed to produce any positive results that can be recorded on film. Visual observation seems to indicate that optical path changes of one fringe can be obtained at the above levels in samples having high surface absorption. Such small changes have been observed in a 3.5 mm thick polycrystalline KCl sample with an abnormally high absorption coefficient (β = 0.02cm^{-1}, believed to be mostly surface absorption). The sample had a square cross section of 2.5cm on the side. The temperature rise measured at the edge when the fringe shift was observed was ~13°C. Our inability to photograph this small change was due to the blurring produced by a combination of speckle noise and fringe localization away from the sample. Nevertheless, even the changes observed visually appear smaller than might be expected from the measured temperature rise at the edge.

Attempts to understand the optical behavior of KCl during irradiation have taken the following directions:

(1) Efforts have been started to eliminate the fringe localization problem by using a holographic recording medium that can be developed in-situ, thereby eliminating any possibility of mis-registration of the hologram plate. This should make it possible to photograph interferograms at lower F-stops and decrease the speckle noise.

(2) Experiments have been performed on the optical distortion of a quartz window irradiated with a CO_2 laser to test the holographic interferometer. The results obtained are described below.

(3) A calculation has been started of the temperature distribution in a window irradiated with a CO_2 laser. The results, which are discussed in subsection IIID, will be used to assess the effect of thermal parameters on the temperature distribution produced by irradiation and in the interpretation of the air calorimeter measurements.

A number of experiments have been conducted using a quartz sample to test the interferometric technique and to compare the temperature rise measured by the interferometric method with those obtained from a measurement of edge temperature with the differential thermocouple. Figures III-5 and III-6 show the time development of the changes in optical thickness of a 1mm thick x 1 inch dia. quartz window that is being irradiated with 2 watts from a laser beam focused by a 30cm focal length Irtran-2 lens to a spot of approximately .75mm in dia. ($\sim$450 w/cm^2). Quartz is used because it is very opaque at 10.6μm so that it can be easily heated with the CO_2 laser; also, its optical properties at the 6328Å wavelength of the interferometric measurements are very well known. In Figure III-5, the hologram plate had been purposely tilted about a vertical axis to introduce a uniform fringe pattern across the sample for use as reference. The times shown in the figures are the length of exposure to the CO_2 laser beam at the time that each photograph was taken (the exposure time for the photograph was 1/10 sec). While it is clear that deformation is taking place, it is also obvious that the introduction of a rectangular fringe-pattern bias on the circularly-symmetric laser-induced deformation makes the interpretation of the fringes difficult. In Figure III-6, the hologram has been brought back to its original position and the entire field contains no fringes. As the laser beam heats the quartz window after different lengths of exposure, one can see the deformation proceeding uniformly with circular symmetry about the beam axis. It can be seen from the photograph that the steady state deformation after a long exposure corresponds to approximately 3.5 fringes. When this measurement was made the temperature rise at the edge of the window, as measured by the differential copper-

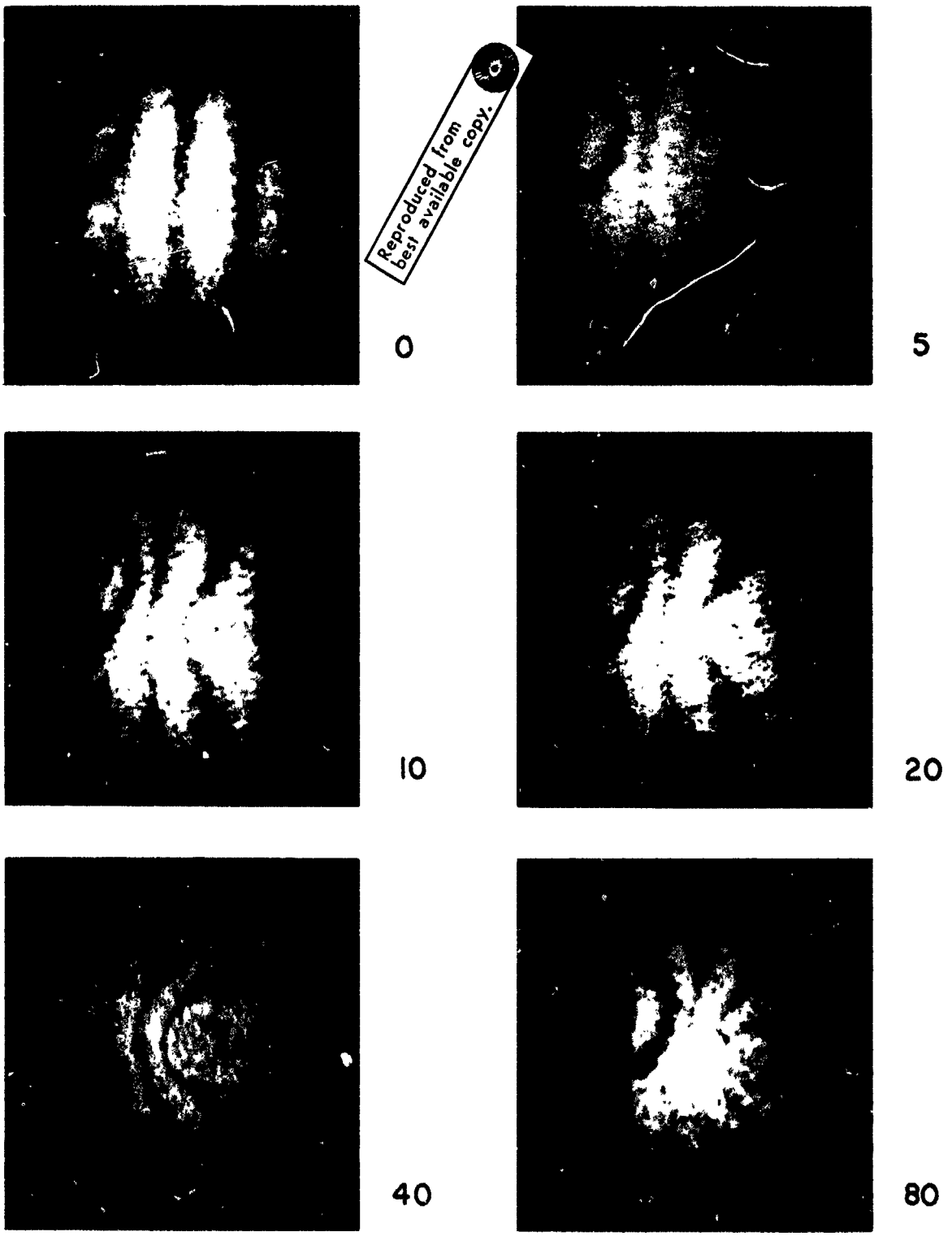

Figure III-5. Change in Optical Thickness of 1mm thick quartz window irradiated with CO_2 laser beam. Hologram tilted about vertical axis. Exposure time shown in seconds.

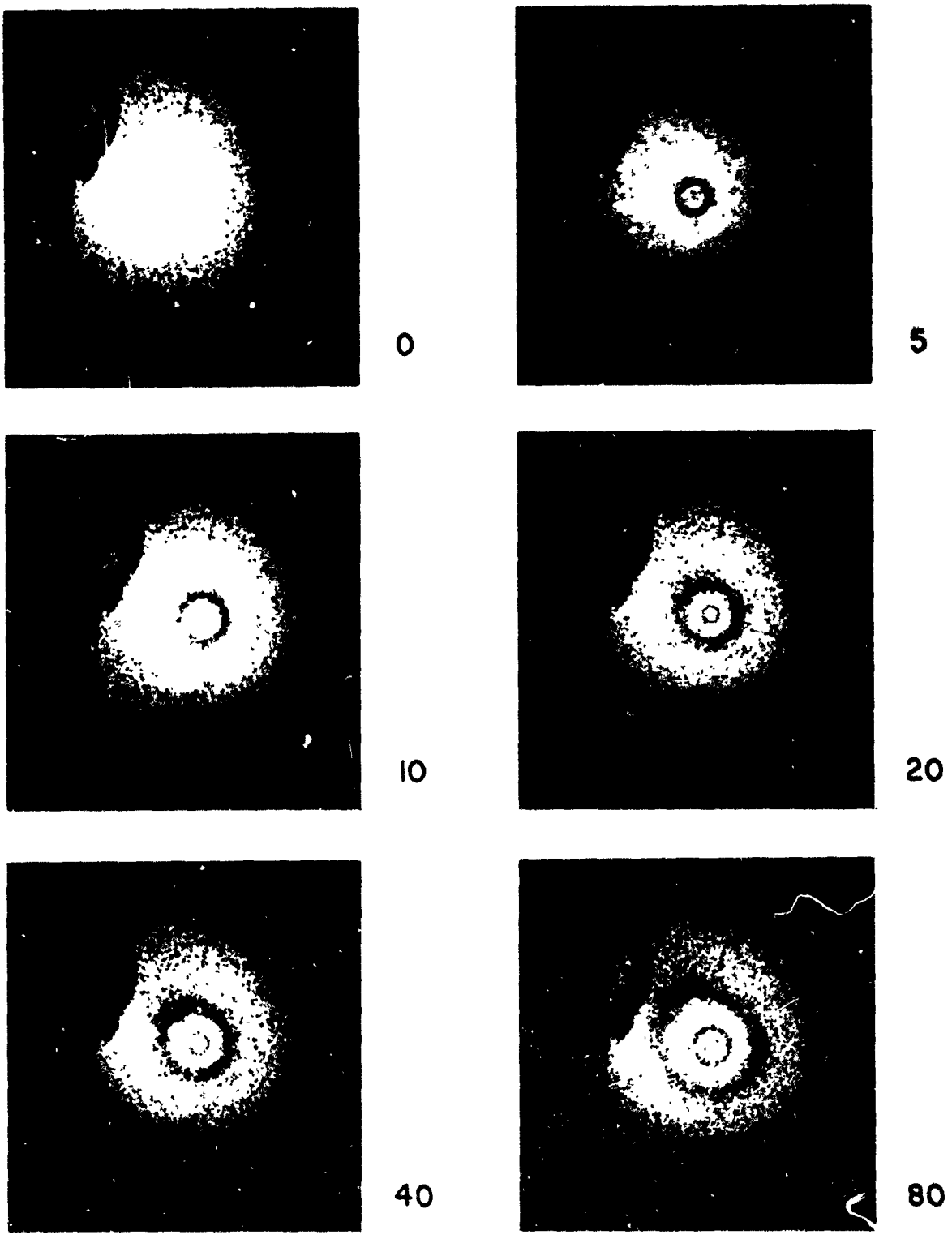

Figure III-6. Change in Optical Thickness of 1mm thick quartz window irradiated with CO_2 laser beam. Exposure time shown in seconds.

constantan thermocouple, was 18°C. As mentioned before, the very pronounced speckle pattern seen in both Figure III-5 and III-6 result from the fact that the fringe pattern is not localized at the object and a very large F number (F/36) had to be used to record both the fringe pattern and the window in focus. A feature in the window that can be used for spatial reference is the shadow of the thermocouple wire attached to the edge of the sample which is seen in the upper left side of the pictures.

Qualitatively, it is important to note that the steady state temperature distribution with the laser on is that shown in the last frame of Figures III-5 and III-6. This temperature is far from uniform, as might be expected, because the beam is localized in a very small area of the sample. When the laser is turned off, the fringe pattern reverses its development during heating, again showing that the sample cools with a nonuniform temperature distribution. These observations on quartz are not directly applicable to halides because of their differences in thermal diffusivities and absorption coefficients. However, they do illustrate the fact that the steady state as well as the transient heating and cooling of a large window irradiated with a small diameter beam can be very nonuniform. Thus, it seems that comparisons of absorption coefficients measured calorimetrically in samples with different thermal diffusivities will require some form of normalization. Also, calorimetric measurements made with the CO_2 laser beam at different distances from the thermocouple may be expected to produce different results.

To obtain quantitative results from the interferograms of Figure III-6, we let the total path length between diffuser and hologram in Figure III-4 be L in the ray approximation. Then

$$L = (\ell - t) + nt = \ell + (n-1)\, t \qquad (3)$$

where ℓ = physical distance from diffuser to hologram

n = refractive index of sample

t = sample thickness

and, ignoring stress effects,

$$\frac{\partial L}{\partial T} = (n-1)\frac{\partial t}{\partial T} + t\frac{\partial n}{\partial T}$$

using $\alpha = \frac{1}{t}\frac{\partial t}{\partial T}$ = linear expansion coefficient

$$\frac{\partial L}{\partial T} = \left[(n-1)\,\alpha + \frac{\partial n}{\partial T}\right]t \tag{4}$$

Now, since we know that one fringe corresponds to a path difference of $\lambda/2$, we define

$$N = \frac{\lambda t}{2\frac{\partial L}{\partial T}} = \frac{\lambda}{2\left[(n-1)\,\alpha + \frac{\partial n}{\partial t}\right]} \tag{5}$$

which is the thickness-temperature-rise product per fringe. This quantity is an intrinsic property of the material, independent of geometry. It can be used to extract the temperature rise corresponding to the nth fringe of an interferogram by using

$$\Delta T = \frac{|N|n}{t} \quad . \tag{6}$$

Table III-1 summarizes some properties of quartz and KCl that are useful to discuss the interferometric results at λ = 6328Å.

Table III-1. Quartz and Potassium Chloride Properties

Property	Quartz	KCl
n	1.457	1.488
$\alpha(^{o}C^{-1})$	0.55×10^{-6}	35.7×10^{-6}
$\frac{\partial n}{\partial T}$ $(^{o}C^{-1})$	1×10^{-5}	-3.4×10^{-5}
$N^{\dagger}$ $(\frac{^{o}K \ cm}{\text{fringe order}})$	3.1	-1.9
κ $(\frac{cm^2}{sec})$	.009	.052
t_d * (sec)	45	7.8
$\beta(cm^{-1})$	>150	.001 - .02

† for λ = 6328Å

* diffusion time across a = 1.25cm. Obtained from $\frac{a^2}{4\kappa t_d} = 1$.

Using the value of N in the table, we find that for the 1mm thick quartz sample of Figure III-6, each full fringe represents a temperature rise ΔT = 31°C. Hence, the peak temperature rise at the center of the window is ΔT ~110°C. Similarly, for the 3.5mm thick sample of KCl discussed earlier in this section, each fringe would result from a temperature rise ΔT = 5.4°C. Thus, our visual observation of one fringe in the KCl sample would correspond to a temperature rise at the center of ~11°C, which is lower than the measured temperature rise ΔT = 13°C at the edge of the sample. Now, from Table III-1 it is clear that the time constant for heat diffusion in KCl is much shorter than it is in quartz; hence, one would not

expect as large a temperature difference between the center and the edge in KCl as is found in quartz. Nevertheless, the temperature at the center, where the laser beam impinges, must obviously be higher than it is at the edge.

It is clear that the interferometric results in KCl require further study. It is very likely that the stress terms in the optical path change cannot be neglected. This work will continue in the next quarter. One of the questions that needs to be resolved is the expected sensitivity of the interferometric method in fringes per watt/cm^2 for a material of a given absorption coefficient β and specified thermal properties. This knowledge will determine a lower limit to the optical flux density required at 10.6μ to produce measurable changes in the optical thickness.

D. CALCULATION OF TEMPERATURE DISTRIBUTION

Knowledge of the temperature distribution produced by irradiation of a sample with a CO_2 laser beam is important to the interpretation of both interferometric and calorimetric measurements. This subsection presents a calculation of the temperature rise produced during a typical experiment in either the interferometer or calorimeter.

The case of interest is one in which a rectangular parallelepiped

$$\left\{0 \leq x_i \leq a_i = 1, 2, 3\right\}$$

is heated by a Gaussian laser beam propagating parallel to x_3 and centered at

$$x_1 = a_1/2,\ x_2 = a_2/2\ .$$

As the beam propagates through the material of absorption coefficient β, its intensity is given by:

$$I(x_1, x_2, x_3) = \frac{4nP_o}{\pi w^2(n^2+1)} \exp\left\{-\frac{2}{w^2}\left[\left(x_1 - \frac{a_1}{2}\right)^2 + \left(x_2 - \frac{a_2}{2}\right)^2\right] - \beta x_3\right\} \quad (7)$$

where

P_o = incident power

n = refractive index

w = Gaussian beam radius.

The power absorbed per unit volume, Q, is

$$Q(x_1, x_2, x_3) = -\frac{\partial I}{\partial x_3} = \frac{4n\, P_o\, \beta}{\pi w^2(n^2+1)} \exp\left\{-\frac{2}{w^2}\left[\left(x_1 - \frac{a_1^2}{2}\right) + \left(x_2 - \frac{a_2^2}{2}\right)\right] - \beta x_3\right\} \quad (8)$$

Assuming that the material loses heat to the environment according to Newton's Law of cooling (for small temperature rise this law describes radiative as well as convective losses), one has at each surface

$$-k \left.\frac{\partial T}{\partial x_i}\right|_{\text{surface}} = hT \qquad i = 1,2,3$$

where T = temperature rise

h = heat transfer coefficient.

The boundary value problem to be solved then becomes,

$$\nabla^2 T + \frac{Q}{k} = \frac{1}{\kappa}\frac{\partial T}{\partial t} \qquad 0 \le x_i \le a_i \qquad i = 1,2,3$$

$$-k\frac{\partial T}{\partial x_i} + hT = 0 \qquad x_i = 0 \qquad i = 1,2,3 \quad (9)$$

$$k\frac{\partial T}{\partial x_i} + hT = 0 \qquad x_i = a_i \qquad i = 1,2,3$$

$$T(x_i, x_2, x_3, t = 0) = 0$$

The solution of this problem can be obtained by the method of finite Fourier transorms[14]. The result is

$$T(x_1, x_2, x_3, t) = \frac{\kappa}{k} \sum_{r,m,n} Z(\alpha_{1r}, x_1) Z(\alpha_{2m}, x_2) Z(\alpha_{3n}, x_3) \exp\left[-\kappa(\alpha_{1r}^2 + \alpha_{2m}^2 + \alpha_{3n}^2)t\right] \lambda \tag{10}$$

$$\int_o^t \exp\left[\kappa(\alpha_{1r}^2 + \alpha_{2m}^2 + \alpha_{3n}^2)t'\right] Q(\alpha_{1r}, \alpha_{2m}, \alpha_{3n}, t')dt'$$

where

$$Z(\alpha_{ij}, x_i) = \frac{\sqrt{2}\left[\alpha_{ij}\cos(\alpha_{ij}x_i) + H\sin(\alpha_{ij}x_i)\right]}{\left[(\alpha_{ij}^2 + H^2)a_i + 2H\right]^{1/2}} \tag{11}$$

$$H = \frac{h}{k} \tag{12}$$

and the α_{ij} are the roots of the transcendental equation,

$$\tan(\alpha_{ij}a_i) = \frac{2\alpha_{ij}H}{\alpha_{ij}^2 - H^2} \tag{13}$$

$$\bar{Q}(\alpha_{1r}, \alpha_{2m}, \alpha_{3n}, t) = \int_o^{a1}\int_o^{a2}\int_o^{a3} Q(x_1, x_2, x_3, t) Z(\alpha_{1r}, x_1) Z(\alpha_{2m}, x_2) \tag{14}$$

$$Z(\alpha_{3n}, x_3)dx_1 dx_2 dx_3.$$

For a typical calorimetric of interferometric measurement, the time dependence of Q is of the form

$$Q(t) = \begin{cases} Q_o & O \le t_1 \le t \\ O & t > t_1 \end{cases} \qquad (15)$$

then

$$\overline{Q}(\alpha_{1r}, \alpha_{2m}, \alpha_{3n}, t) = \frac{4nP_o\beta}{n^2+1} \sqrt{\frac{2}{[(\alpha_{1r}^2+H^2)\alpha_1+2H][(\alpha_{2m}^2+H^2)a_2+2H][(\alpha_{3n}^2+H^2)a_3+2H]}}$$

$$x \frac{\exp[-\frac{w^2}{8}(\alpha_{1r}^2+\alpha_{2m}^2)]}{\beta^2+\alpha_{3n}^2} \cdot \left\{ \alpha_{1r} \cos\left(\frac{\alpha_{1r} a_1}{2}\right) + H \sin\left(\frac{\alpha_{1r} a_1}{2}\right) \right\}$$

$$x \left\{ \alpha_{2m} \cos\left(\frac{\alpha_{2m} a_2}{2}\right) + H \sin\left(\frac{\alpha_{2m} a_2}{2}\right) \right\} \left\{ \alpha_{3n}(\beta+H) + e^{-\beta a_3} \left[(\alpha_{3n}^2 - H\beta) \sin(\alpha_{3n} a_3) \right] \right.$$

$$\left. - (\beta+H)\alpha_{3n} \cos(\alpha_{3n} a_3) \right\} \left\{ \mathrm{Re}\left[\mathrm{erf}\left(\frac{a_1}{w\sqrt{2}} - i \frac{\alpha_{1r} w}{2\sqrt{2}}\right)\right] - \mathrm{Re}\left[\mathrm{erf}\left(-i \frac{\alpha_{1r} w}{2\sqrt{2}}\right)\right] \right\}$$

$$\left\{ \mathrm{Re}\left[\mathrm{erf}\left(\frac{a_2}{w\sqrt{2}} - i \frac{\alpha_{2m} w}{2\sqrt{2}}\right)\right] - \mathrm{Re}\left[\mathrm{erf}\left(-i \frac{\alpha_{2m} w}{2\sqrt{2}}\right)\right] \right\}$$

where $i = \sqrt{-1}$

After performing the time integration in (10), one obtains

$$T(x_1, x_2, x_3, t) =$$

$$\frac{1}{k} \sum_{r,m,n} \frac{Z(\alpha_{1r}, x_1) Z(\alpha_{2m}, x_2) Z(\alpha_{3n}, x_3) \overline{Q} \left\{1 - \exp\left[-\kappa(\alpha_{1r}^2 + \alpha_{2m}^2 + \alpha_{3n}^2)t\right]\right\} t \le t_1}{\alpha_{1r}^2 + \alpha_{2m}^2 + \alpha_{3n}^2}$$

$$\frac{1}{k} \sum_{t,m,n} \frac{Z(\alpha_{1r}, x_1) Z(\alpha_{2m}, x_2) Z(\alpha_{3n}, x_3) \overline{Q} \left\{\exp\left[\kappa(\alpha_{1r}^2 + \alpha_{2m}^2 + \alpha_{3n}^2)t_1\right] - 1\right\}}{\alpha_{1r}^2 + \alpha_{2m}^2 + \alpha_{3n}^2} \times$$

$$\exp\left[-\kappa(\alpha_{1r}^2 + \alpha_{2m}^2 + \alpha_{3n}^2)t\right] \qquad t > t_1 \qquad (17)$$

where $\overline{Q}$ is given by (15) and erf $(x+iy)$ is the complex error function (15).

A computer program is being written to evaluate the temperature distribution function (17). In spite of the complex appearance of Equation (17), this is a straightforward procedure, assuming no convergence problems. In fact, the roots α_{ij} increase by $\sim \pi$ for each increment of j, so we expect that only a few terms will be needed to obtain reasonable accuracy. The main difficulties in evaluating each summand are associated with the procedures for finding the roots of (13) and evaluating the complex error function, both of which have already been programmed and tested.

The heat transfer coefficient, h, in the above calculation is a quantity that represents a linearized approximation to the heat loss from the surface of the solid. For a window of a few inches in cross-section positioned vertically in still air and a temperature rise of $\sim 10°C$, the coefficient is $h \sim 8 \times 10^{-4}$ watts/cm^2 °C. For the same sample in vacuum, the heat loss is by radiation. Then, for small temperature excursions

$$h \simeq 4 \epsilon \sigma T_o^3$$

where ϵ = emissivity

σ = Stefan-Boltzman constant

T_o = ambient temperature in °K

Assuming T_o = 300°K, one obtains

$$h \tilde{-} 6.19 \times 10^{4} \epsilon \text{ watts/cm}^2 \text{°K}$$

Now, since emittance equals absorptance and for halides the later is $\sim 10^{-3}$

$$h \sim 6 \times 10^{-7} \text{ watts/cm}^2 \text{°K}$$

Thus, in the vacuum colorimeter one approaches the condition of no heat flow at the boundary.

The results of the calculation will be used to interpret interferometric results, and to examine questions concerning the interpretation of calorimetric measurements. The method of finite Fourier transforms can be equally well applied to round windows.

SUMMARY

In this report we have reviewed the mechanism of high temperature deformation of halides. We have shown that it is possible to arbitrarily deform halides without introducing voids. We then described processes such as extrusion, forging and rolling and equipment used in our program for hot working of these materials.

The microstructural characteristics, strength and aging were described. It was shown that stable, small grained structures of high strength can be produced by forging. However, excessive deformation can produce unstable structures that exhibit abnormal grain growth at room temperature.

The techniques and equipment used to measure optical absorption and laser-induced changes in optical path in alkali halides were described. The polycrystalline materials exhibit absorption coefficients comparable to the single crystals. The interferometric measurements of laser-induced distortion in polycrystalline potassium chloride are not well understood. However, measurements of distortion, of a fused quartz window during laser irradiation raise some questions regarding the interpretation of calorimetric measurements. A calculation of the temperature rise in a low-absorption material to be used in the interpretation of interferometric and calorimetric results is given.

FUTURE PLANS

The processing studies in the next quarter will shift the emphasis to rolling of single crystal and polycrystalline ingots. The microstructures, textures and strength of rolled materials will be studied.

The holographic interferometry will be improved and its sensitivity to laser-induced deformation will be determined. The effect of localized laser irradiation on the microstructure will be examined. Measurements of stress-birefringence, which are currently in a very early stage, will be refined and scattering measurements will be started.

REFERENCES

(1) R. J. Stokes, Proc. Brit, Ceram. Soc. 6, 189 (1966).

(2) G. W. Groves and A. Kelly, Phil. Mag. 8, 877 (1963).

(3) J. J. Gilman, Acta. Met. 7, 608 (1959).

(4) R. B. Day and R. J. Stokes, J. Am. Ceram. Soc. 49, 72 (1966).

(5) S. Amelinckz, "Dislocations and Mechanical Properties of Crystals", Wiley, New York (1957).

(6) E. Bernal G., B. G. Koepke, R. H. Anderson, R. J. Stokes, Quarterly Technical Report No. 1 on Contract No. DAHC15-72-C-0227, April - June 1972.

(7) N. J. Grant, et al., Research on Materials for High Power Lasers, Quarterly Report No. 1, M.I.T., 15 Aug 1972.

(8) R. W. Rice, N.B.S. Special Publ. 348, p. 365 (1972).

(9) F. Horrigan, C. Klein, R. Rudko, D. Wilson, "Windows for High Power Lasers", Microwaves, p. 68, Jan 1969.

(10) Quarterly Report 5, LQ-10 Program, AFCRL-72-0339, 22 May 1972.

(11) American Institute of Physics Handbook, 2nd Edition, D. Gray, editor, McGraw-Hill, New York, N.Y. (1963).

(12) H. M. Smith, "Principles of Holography", Wiley, New York, N.Y. (1969).

(13) R. J. Collier, C. B. Burckhardt and L. H. Lin, "Optical Holography", Academic Press, New York N.Y. (1971).

(14) M. N. Ozisik, "Boundary Valve Problems of Heat Conduction", Intext, Scranton, Pa. (1968).

(15) Handbook of Mathematical Function, M. Abramovitz and I. A. Stegun, editors, U. S. National Bureau of Standards AMS55, U. S. Government Printing Office, Washington, D. C. (1966).